NASA CR 137951

A NUMERICAL STUDY OF THE TEMPERATURE FIELD IN A COOLED RADIAL TURBINE ROTOR

BY

A. HAMED, E. BASKHARONE AND W. TABAKOFF

(NASA-CR-137951) A NUMERICAL STUDY OF THE TEMPERATURE FIELD IN A COOLED RADIAL TURBINE ROTOR Interim Report (Cincinnati Univ.) 71 p HC A04/MF A01 CSCL 21E

N77-20107

Unclas
G3/07 22616

Supported by:

NATIONAL AERONAUTICS AND SPACE ADMINISTRATION

Ames Research Center

U.S. Army Air Mobility Research & Development Laboratory

Moffett Field, California

Contract No. NAS2-7850

NASA CR 137951

A NUMERICAL STUDY OF THE TEMPERATURE FIELD IN A COOLED RADIAL TURBINE ROTOR

by

A. Hamed, E. Baskharone and W. Tabakoff

Supported by:

NATIONAL AERONAUTICS AND SPACE ADMINISTRATION

Ames Research Center

U.S. Army Air Mobility Research & Development Laboratory

Moffett Field, California

Contract No. NAS2-7850

1. Report No.	2. Government Accession No.	3. Recipient's Catalog No.
NASA CR 137951		

4. Title and Subtitle	5. Report Date
A NUMERICAL STUDY OF THE TEMPERATURE FIELD IN A COOLED RADIAL TURBINE ROTOR	March 1977
	6. Performing Organization Code
7. Author(s)	8. Performing Organization Report No.
A. Hamed, E. Baskharone and W. Tabakoff	
	10. Work Unit No.
9. Performing Organization Name and Address	11. Contract or Grant No.
Department of Aerospace Engineering & Applied Mechanics University of Cincinnati Cincinnati, Ohio 45221	NAS2-7850
	13. Type of Report and Period Covered
12. Sponsoring Agency Name and Address	Contractor Report
National Aeronautics & Space Administration Washington, D.C. 20546 and U.S. Army Air Mobility Research & Development Laboratory Moffett Field, California 94035	14. Sponsoring Agency Code

15. Supplementary Notes

Interim Report. Project Manager, LTC Dwain Moentmann, U.S. Army Air Mobility Research and Development Laboratory, Ames Research Center, Moffett Field, California 94035.

16. Abstract

In this work, the three dimensional temperature distribution in the cooled rotor of a radial inflow turbine is determined numerically using the finite element method. Through this approach, the complicated geometries of the hot rotor and coolant passage surfaces are handled easily, and the temperatures are determined without loss of accuracy at these convective boundaries. Different cooling techniques with given coolant to primary flow ratios are investigated, and the corresponding rotor temperature fields are presented for comparison. The data obtained from the present analysis were found to be in agreement with the available experimental measurements.

The present work can be used in combination with a finite element stress analysis to investigate the thermal stresses corresponding to the different cooling arrangements. This can provide valuable information concerning the critical locations of possible creep, rupture or fatigue, for a given centrifugal, thermal and aerodynamic loading.

17. Key Words (Suggested by Author(s))	18. Distribution Statement
Turbomachinery Cooling Radial Turbine	Unclassified - unlimited

19. Security Classif. (of this report)	20. Security Classif. (of this page)	21. No. of Pages	22. Price*
Unclassified	Unclassified	67	

* For sale by the National Technical Information Service, Springfield, Virginia 22161

TABLE OF CONTENTS

SUMMARY

In this work, the three dimensional temperature distribution in the cooled rotor of a radial inflow turbine is determined numerically using the finite element method. Through this approach, the complicated geometries of the hot rotor and coolant passage surfaces are handled easily, and the temperatures are determined without loss of accuracy at these convective boundaries. Different cooling techniques with given coolant to primary flow ratios are investigated, and the corresponding rotor temperature fields are presented for comparison. The data obtained from the present analysis were found to be in agreement with the available experimental measurements.

The present work can easily be used in combination with a finite element stress analysis, to investigate the thermal stresses corresponding to the different cooling arrangements. This can provide valuable information concerning the critical locations of possible creep, rupture or fatigue, for a given centrifugal, thermal and aerodynamic loading.

INTRODUCTION

The radial inflow turbines offer many advantages over axial flow turbines in small gas turbine applications. Besides operating at higher efficiency and yielding greater temperature drop and pressure ratio per stage, the radial inflow turbine rotor can be cast at a relatively low cost. Further improvements in gas turbine engine efficiencies require increased gas temperatures at the turbine inlet. As a result of metallurgical limitations, higher gas stream temperatures can be permitted without reducing the allowable stress levels through effective cooling of the turbine rotor.

The various aspects of axial flow turbine cooling have been thoroughly investigated and the different techniques adequately developed. Several experimental and theoretical studies dealing with axial flow turbine cooling can be found in the literature. The merits and limitations of the different cooling techniques, namely convection, transpiration, and film cooling are discussed in Reference [1]. Most internal cooling systems have been designed using semi-empirical methods to achieve the highest possible effectiveness. Reference [2] presents a review of the present state of the art for the internal cooling of turbine nozzles in aircraft applications.

Although radial turbine development, has progressed up to the limits of stress operating conditions, its rotor cooling did not achieve the high level of sophistication accomplished in the axial turbines. As a matter of fact, until recently very little research work has been reported dealing with radial inflow turbine rotors. Branger [3] investigated experimentally the effectiveness of veil cooling the hub side of the rotor. He found that the cooling effectiveness was larger at the rotor tip, and decreased as the cooling film is heated and mixed with the hot turbine flow. Petrick and Smith [4] measured the temperatures of a radial inflow turbine rotor which was cooled from its backside. While veil and

rotor backside cooling techniques are effective for the rotor disk, they induce little variation in the blade temperature. Therefore, except for very highly conducting rotor materials, only internal cooling can produce pronounced reduction in the blade temperatures as reported in Reference [5].

Due to the high cost and difficulties associated with experimental studies, computational methods can be developed to provide valuable information about the temperature and the stress distributions resulting from the different cooling techniques. In the present study a numerical method is developed to determine the temperature field in the rotor of the radial inflow turbine. The computations are based on the use of the finite element method, with a variational statement of the three dimensional conduction problem. The boundary conditions involved at the different external and internal cooling surfaces of the rotor which is shown schematically in Figure 1, are discussed. Different cooling methods and coolant flow rates are investigated and the resulting cooling effectiveness and temperature distributions are reported.

ANALYSIS

The blade temperature distribution in axial flow turbines is often predicted from two dimensional computations at radial stations. Any radial variation in temperature accounts only for the spanwise variation in the overall convective heat transfer coefficient but not the spanwise conduction. In the case of radial inflow turbines, a similar approach cannot be used due to its complex geometry. The rotor temperature distribution must therefore be evaluated using three dimensional heat transfer analysis.

In choosing a thermal analyzer for use in the case of the radial inflow turbine rotor, several factors such as nodal point placement, input efficiency, accuracy, storage requirements, and computer time must be taken into consideration. While the three dimensional finite difference thermal analyses are basically first order accurate, the finite element method offers the advantage of the capability of altering the basic accuracy

of the method. The finite element method was used in this study because of the advantages it offers in terms of input efficiency and nodal point placement. This is particularly important in the temperature computations of turbine rotors with internal cooling passages. Furthermore, the stress analysis of the turbine rotor using any of the commercially available finite element programs, can be greatly facilitated by using a thermal analyzer such as the one presented here. In the following, the governing equations are derived from variational principles.

Governing Equations

The field equation for the steady state three dimensional heat conduction problem in an isotropic medium can be expressed as:

$$\nabla\cdot(k\nabla T) + g = 0 \tag{1}$$

where T is the temperature, k the coefficient of thermal conductivity, and g the heat generation rate per unit volume. The boundary conditions associated with the problem under consideration are:

$$k\nabla T \cdot \bar{n} + h(T - T_\infty) = 0 \quad \text{on} \quad S_h \tag{2}$$

and

$$k\nabla T \cdot \bar{n} + q = 0 \quad \text{on} \quad S_q \tag{3}$$

In the above equations, h denotes the convective heat transfer coefficient on the surface S_h, which convects heat to the flow at temperature T_∞, and q is the specified heat flux density on the surface S_q. The union of S_h and S_q forms the complete surface boundary S, whose outward normal unit vector is $\bar{n}$.

The partial differential equation (1) and its boundary conditions (2) and (3) can be cast in the following variational form according to References [6] and [7].

$$I(T) = \frac{1}{2}\int_V \left[k\left(\frac{\partial T}{\partial x}\right)^2 + k\left(\frac{\partial T}{\partial y}\right)^2 + k\left(\frac{\partial T}{\partial z}\right)^2 - 2g\ T\right]dV$$

$$+ \int_{S_h} \left(\frac{1}{2} h\ T^2 - h\ T_\infty T\right)dS + \int_{S_q} q\ T\ dS \qquad (4)$$

where the desired temperature field $T(x,y,z)$ minimizes the functional "I" over the domain of interest:

$$\delta(I) = 0 \qquad (5)$$

Boundary Conditions:

The formulation of the governing equations has been kept very general up till now. The surface integral was intentionally divided into two parts, one for the boundary surfaces over which a known amount of heat flux is specified and the second over the rest of the boundary surface convecting heat to a gas of known temperature. In the following section, the conditions associated with the different rotor boundaries will be discussed and the empirical expressions for the main and coolant convective heat transfer coefficients will also be given.

Due to its rotation, any circumferential nonuniformity in the flow conditions at inlet to the rotor will be relatively averaged out, and therefore it was assumed that the inlet flow is axisymmetric. The rotor shown in Figure 1 was divided into a number of wedge sections equal to the number of blades. It will be sufficient to determine the temperature in any one of these sections since, with the assumption of axisymmetric inlet and exit flow conditions, the temperature field will be periodic. One rotor section is shown in Figure 2, with one rotor blade at the middle. The heat transfer was assumed to be negligible at the rim. With the small temperature differences between the blades pressure and suction side, it is also reasonable to assume that the heat exchange by conduction between two adjacent sections is negligible. Therefore, in the

problem formulation (Eq. 4) the heat flux q was taken as zero on the surface S_q consisting namely of the rim and the two sides of the rotor section of Figure 2. The rest of the surfaces of the rotor section will be subjected to the hot gas flow.

Main Stream Convection

The local convective heat transfer coefficient between the blade and the main stream depends on the blade shape, the gas velocity and the position of the boundary layer transition point. The highest heat transfer coefficient is found at the blade leading edge, where the laminar boundary layer is thin, its value is determined from the following formula for transverse flow over cylinders [8].

$$Nu = 1.61\ Pr^{0.4}\ Re^{0.5} \tag{6}$$

where Nu is the Nusselt number, Pr is the Prandtl number and Re is the Reynolds number based on the relative free stream velocity and the blade leading edge radius.

Ainley [9] found that the mean heat transfer coefficients of rotating turbine blades were much higher than those for the same blades in two dimensional cascades. This can be attributed to the strong turbulence in the main flow of turbines. Therefore, turbulent boundary layer formulation was used in the present study for calculating the convective heat transfer coefficient between the rotor and the hot gas. This will lead to conservative estimates of heat transfer coefficients, resulting in higher predicted metal temperatures, but will be used until more knowledge of the flow behavior in the turbine rotor becomes available. The following expression for the Nusselt number was used throughout the course of this investigation:

$$Nu = \frac{Pr\ Re\ (C_f/2)^{0.5}}{(2/C_f)^{0.5}+5\{(Pr-1)+\ln[1+0.83(Pr-1)]\}} \tag{7}$$

Where the friction coefficient, C_f, is evaluated using the following empirical correlation for flat plate:

$$C_f = 0.0576\ Re^{-0.2} \qquad (8)$$

In the case of a cooled rotor, the rest of the convective boundary conditions will depend on the particular cooling arrangement under consideration. These will be discussed in the following section dealing with rotor cooling.

Rotor Cooling:

Because of the high centrifugal accelerations experienced by the rotor blades, they are cooled to lower metal temperatures when compared to the nozzle blades. Due to their motion relative to the hot gas however, the adiabatic wall temperatures recovered on the rotor surfaces will be lower, and furthermore any higher temperatures in the gases leaving the burner above the mean values will be averaged out circumferentially at inlet to the rotor. Creep life consideration requires an accurate determination of the rotor temperature distribution.

While several experimental and theoretical investigations of turbine blade cooling can be found in the literature, very few investigators were concerned with radial inflow turbine rotor. Experimental investigations of external rotor cooling can be found in References [3] and [4]. In the experimental study of Branger [3], the hub side of the radial rotor was veil cooled. It was found that veil cooling is more effective near the rotor tip before the cooling film is heated and mixed with the hot stream. Petrick and Smith [4] measured the rotor temperatures when its backside is externally cooled by radially outward, radially inward flows and by normal impingement. They found that the normal impingement resulted in the highest cooling effectiveness while the radial inflow of coolant on the rotor backside gave the poorest results.

While both rotor backside and veil cooling are effective in cooling the rotor disk, they induce little variation in the

blade temperatures for the metals normally used in rotor manufacturing. Therefore, unless highly conducting rotor materials are used, internal cooling passages in the rotor blades are used to obtain the desired blade temperature reduction. In this study the rotor temperature distribution is determined for the different cooling techniques shown in Figure 3. The first three configurations show different internal cooling arrangements. The radial narrow holes provide the cooling passage in 3A. In the second arrangement 3B, which will be referred to thereafter as the single path, the coolant is introduced near the hub from the rotor backside, proceeds inside the blade and is discharged at the rotor tip. The cooling configuration C, will be referred as the double path. In this case the coolant is introduced at the rotor end opposite its backside, cools the blade internally, turning around at the leading edge, then is discharged at the blade suction side. One external cooling scheme is also investigated, which is shown schematically in Figure 3D. In the following sections, the coolant temperature computations and empirical expressions used for the coolant convective heat transfer coefficient will be discussed.

Internal Cooling:

The flow in the internal cooling passages is affected by the centrifugal and the Coriolis forces. Miyazaki [10] found that the secondary flow is especially suppressed when the cross-sectional aspect ratios are further from unity. Under these conditions, the Nusselt number was very close to that in stationary straight pipes having the same hydraulic diameter. The average Nusselt number for fully developed turbulent flow at high temperatures and heat flux densities is expressed, according to Reference [11], as:

$$Nu = \frac{hD}{k} = 0.034(D/L)^{0.1} Pr^{0.4} Re^{0.8} (T_c/T_s)^{0.8} \quad (9)$$

where D is the hydraulic diameter, L the passage length, T_c and T_s are the coolant and hot passage temperatures respectively. Both Nusselt and Reynolds numbers are based on the hydraulic diameter, and the flow properties are referenced to T_s.

External Cooling:

Petrick and Smith [4] experimentally investigated the radial turbine rotor backside cooling by air flowing parallel to the disk in both radially inward and radially outward directions as well as by air impinging perpendicular to the disk. They found that the radially outward flow resulted in higher values of convection heat transfer coefficients than the radially inward flow. The coolant flow perpendicular to the disk however, resulted in much higher values of convective heat transfer coefficients compared to those values obtained with flow arrangements parallel to the rotor backside. They also used their experimental measurements to derive empirical expressions for the convective heat transfer coefficient in all three cases. The experimental data of this reference is so scattered that the authors themselves recommended limiting it application only to the range of the parameters in their study.

Experimentally determined average Nusselt number for radially outward flow on a rotating shrouded disk are reported by Haynes and Owen [12]. The influence of the coolant flow rate and the shroud and backside clearances were found to be less pronounced at high rotational Reynolds numbers. The Nusselt number would approach the free rotating disk values for the high speeds and low coolant flow rates which are involved in radial turbine applications. The free disk correlation was therefore used in the present study to determine the local Nusselt number variation along the rotor backside

with the cooling air flowing radially outward. Kreith et al. [13] found that the critical Reynolds number of enclosed rotating disks with source flows is lower than the free disk values. Therefore, neglecting any small laminar core, that can exist on the rotor backside, the local Nusselt number at any radius r, was calculated using the following equation [14]:

$$Nu = \frac{hr}{k} = 0.0195 \left(\frac{\omega r^2}{\nu}\right)^{0.8} \tag{10}$$

where ω is the angular velocity of the rotor, and ν is the kinematic viscosity.

Coolant Temperature Computations:

The temperature of the cooling stream increases along its flow path due to the heat exchange with the hot rotor. This in turn affects the cooled surface temperature as well as the convective heat transfer coefficient. The computations of the rotor and coolant flow temperature distribution must therefore be performed concurrently. The rotor temperature computations are carried out using the finite element formulation of the variational statement for the three dimensional conduction problem. The cooling air temperature is evaluated in a separate program in order to achieve the desired accuracy without significantly increasing the storage requirements of the conduction problem.

A simple energy balance equation was used to determine the coolant temperature rise, ΔT_c, over an incremental length, ΔL, of the passage.

$$\Delta T_c = \frac{P}{\dot{m} C_p} h(T_s - T_c) \Delta L \tag{11}$$

where P is the perimeter of the cooling passage, and $\dot{m}$, the coolant flow rate.

The same procedure was followed in the rotor backside coolant stream, to determine the variation in its temperature over an increment of radius, Δr.

$$\Delta T_c = \frac{2\pi r}{\dot{m} C_p} h(T_s - T_c)\Delta r \qquad (12)$$

The convective heat transfer coefficients in the above equations are evaluated by using equations (9) and (10) respectively.

Finite Element Representation:

The solution domain is discretized into a number of three dimensional finite elements. The temperature variation within each element $T^{(e)}(x,y,z)$, is generally represented by an equation of the form [15]:

$$T^{(e)}(x,y,z) = \{N\}^t \{T\}^{(e)} \qquad (13)$$

Where $\{N\}^t$ is the row vector of the interpolation functions which depend on the nodal coordinates, and $\{T\}^{(e)}$ is the column vector consisting of the nodal values of the temperature associated with that element.

The interpolation functions N_i, are chosen to satisfy continuity requirements to ensure the convergence of the solution. The integral over the whole domain in equation (4) can therefore be represented as the sum of the integrals over all the elements:

$$I = \sum_{e=1}^{e=M} I^{(e)} \qquad (14)$$

where M is the total number of elements in the solution domain.

It is required to stationalize $I(T)$ with respect to all the nodal values of T in the solution domain, however from equation (14) we can write

$$\delta I = \sum_{e=1}^{M} \delta I^{(e)} = 0 \qquad (15)$$

where the variation of $I^{(e)}$ is taken only with respect to the nodal values associated with the individual element (e). This implies that:

$$\frac{\partial I^{(e)}}{\partial T_i} = 0 \qquad i = 1, 2, \ldots r \qquad (16)$$

where r is equal to the number of nodal temperatures per element. It would therefore be necessary to derive only the single element equation.

The simple four node tetrahedral elements, with linear interpolation functions were used in this analysis. This choice was dictated by computer storage considerations. In spite of their simplicity, these elements are very versatile however because of the ease with which they can be assembled to fit the complex three dimensional geometries with reasonable fidelity. A comparison of these elements with other higher representations [16], shows the improvement in accuracy is not great. The derivation of the single element equation for the particular finite element and interpolation function used in this study is given in Appendix A. When these equations for all the elements that constitute the rotor body are assembled, a relation of the following form is obtained:

$$[K] \{T\} = \{R\} \qquad (17)$$

Where [K] is the global stiffness matrix, {T} is the column vector of all the rotor nodal temperatures, and {R} is the column vector of thermal loading. The finite element representation of the rotor section, shown in Figure 2, using the four node tetrahedral elements results in a set of linear equations whose matrix of coefficients has a relatively narrow

band width. It is therefore adequate to solve these equations directly using an algorithm based on Choleski's decomposition [17], forward reduction and backward substitution.

RESULTS AND DISCUSSION

Two previous studies involving external rotor backside cooling and internal blade cooling that could be used to verify the results of this study were available in References [4] and [5]. Although rotor temperature measurements were reported in Reference [3], the turbine geometry and flow data supplied in that study was not sufficient to carry out any flow or heat transfer computations. It was therefore decided to carry out our computations for a rotor and flow conditions similar to that given in Reference [5] except for one difference. The rotor disk was extended up to the blade tip to check the ability of our program to handle such complicated three dimensional geometry.

The rotor is made of IN100, a nickel base high temperature alloy, and its tip diameter is 8.2 inches. The hot gas inlet total temperature is 2225°F at 67,000 rpm and a turbine flow rate of 4.9 lb/sec. In all the cases investigated, the cooling air total temperature at inlet was assumed to be 850°F. The resulting temperature distributions are presented in the form of plots of isothermal lines on the surfaces of the blade and its associated hub section in Figures 4 through 9.

The temperature fields are presented for cooled as well as for uncooled rotors. A schematic of the four different cooling arrangements investigated is shown in Figure 3. The computations were executed on an IBM 370 time sharing system. The computation time depended on the number of nodal points and on the particular internal cooling passage investigated, which in turn affects the band width of the stiffness matrix. For the simpler cases of solid rotor blades, the computer time was 15 seconds. Aside from the uncooled rotor, this includes

the cases of external rotor backside cooling, and the first internal cooling arrangement. With the very narrow cooling passages of that cooling arrangement, heat sinks were introduced to represent the amount of heat absorbed by the coolant in the elements which included any portions of the passages. The discretization of these cases involved 256 nodal points, 675 finite elements. The number of nodal points and elements were larger for the rotor with internal cooling passage, in which the discretization involved the modeling of the coolant passage. The case involving rotor cooling through the single path shown in Figure 3 was modeled using 300 nodal points, and 837 elements. Larger number of nodes and elements, 380 and 1038 respectively, were used in the more complex double path cooling resulting in larger stiffness matrix band width and longer computational time. Additional external convective surface elements and larger stiffness matrix band widths, were naturally involved in the last two cases.

The temperature field in an uncooled rotor is shown in Figure 4. The figure shows two views of the rotor section as seen from the blade pressure and suction sides. As expected, the highest temperatures are found near the rotor tip, and decrease gradually towards the hub. Both centrifugal and aerodynamic loading cause the highest stresses at the blade sections near the hub. The relatively moderate radial temperature gradients of Figure 4 are not expected to contribute significantly to the stress field. Rotor cooling should be expected to reduce the high temperatures of 1550°F near the blade hub. If the radial temperature gradient resulting from a particular cooling arrangement is considerably high, it can augment the stresses produced by centrifugal and aerodynamic loading. These two factors have to be taken into consideration when the different cooling configurations are compared. The losses incurred by the coolant injection after circulating through the particular cooling path is another important factor to be considered [18]. This however is beyond the scope of this study.

Figure 5 shows the isothermal lines for 1.5% internal cooling through the single path in the rotor blades. It is clear that even for this small amount of coolant mass flow, a reduction in the temperatures of 100 to 150°F is achieved in the highly stressed blade regions near the hub. The blade temperatures were computed for the same cooling arrangement in Reference [5], and the resulting temperature fields were given in Figures 81 and 82. When the blade temperatures of Figure 5 are compared with the computed results of Reference [5], lower blade temperatures can be observed in the latter data. We must point out however that, the blade temperatures of Reference [5] were first iterations, calculated assuming zero heat flux at the blade hub. It was mentioned in that reference that the adiabatic blade end wall can account for about 50°F in lower calculated temperatures at the smaller radius hub sections.

The temperature field for 3% internal blade cooling through a double path is shown in Figure 6. In this arrangement, 0.5% cooling is discharged at the tip to avoid choking. The computed rotor temperature field for this cooling arrangement is shown in Figure 6. When the blade temperatures of this figure were compared with those in Figures 89 and 90 of Reference [5], it was found that they are in close agreement. The results of the last reference for this cooling arrangement were obtained after three iterations, to account for the rotor blade end wall heating effect at the hub. It can be seen from Figure 6 that the double path cooling arrangement results in a considerable temperature reduction in the blades highly stressed areas. This temperature reduction is achieved however with large temperature gradients in the blade that can produce considerable thermal stresses.

In the two internal cooling arrangements just described, the lowest metal temperatures can be observed around the area of the coolant introduction in the rotor section. That can explain the considerable reduction in the blade highly stressed regions in the case of a single path cooling even at the

relatively low coolant mass flow of 1.5%. With 3% double path cooling, the temperature reduction was not great, since the coolant is introduced at the opposite side of the rotor, going through a longer path before reaching these regions.

In the third internal cooling arrangement investigated, the coolant path consists of a number of holes drilled radially in the rotor blade. The resulting temperature distribution with 1.5% coolant is shown in Figure 7. It can be seen that this arrangement with five cylindrical cooling passages of 0.06 inch diameter results in the maximum overall reduction in the metal temperature, as well as in the lowest blade temperature near the highly stressed regions. Although this is desirable for better creep life, it is obvious that large radial temperature gradients prevail along the rotor section. Furthermore, large stress concentrations around the narrow radial cooling passages are associated with this arrangement.

Additional results are shown in Figures 8 and 9, which were obtained for 1.5% and 3% external rotor disk backside cooling by radial outflow. It can be observed that the rotor backside temperatures are almost invarient near the axis and up to a radial distance greater than half the tip diameter, then increases sharply towards the tip. The temperature distribution of Figure 9 can be qualitatively compared with the experimental data given in Reference [4] for the corresponding cooling arrangement. Although the ratios of coolant to main flow investigated experimentally in Reference [4] were generally high, the temperature measurements at the lowest coolant mass flow of 4% showed the same tendencies as our temperature field computations.

The cooling effectiveness was computed with 1.5% and 3% cooling mass flow for the rotor disk external cooling arrangement. The effectiveness, η, was defined according to the following expression:

$$\eta = \frac{T_{rh} - T_{rc}}{T_{rh} - T_{c}}$$

Where T_{rc} and T_{rh} are the rotor temperatures with and without cooling, respectively. It can be seen from Figures 10 and 11 that, as expected, the maximum effectiveness occurs at the point of impingement and decreases towards the rotor tip. By comparing Figures 10 and 11 with Figures 8 and 9, it is seen that the effectiveness curves are very similar to the isothermal curves. Therefore, it was unnecessary to present additional figures showing the effectiveness for the other cooling arrangements, since the inlet coolant temperature, T_c, was kept the same in all the cases considered.

If Figures 8, 9 and 4 are compared, it can be seen that the rotor backside cooling is more effective in cooling the rotor disk, but leaves the blade temperatures practically unaffected. Therefore, this cooling arrangement cannot be effective in reducing the blade temperatures except for highly conductive rotor materials. It is clear however that it is advantageous from the stresses point of view since it mainly results in axial temperature gradients. Using rotor backside cooling in combination with internal cooling might therefore offer some advantages. This can be especially true if the internal cooling air is introduced at the rotor backside, as in the case of the single path. In this case, the internal cooling air will pass initially through a rotor section with reduced temperatures caused by the rotor backside cooling. If half of a 3% coolant is used internally in a single path and the other half externally on the rotor backside, for example, considerably lower coolant temperatures can be expected in the internal path near the highly stressed blade regions, just as the coolant passage is enlarged. This combined cooling arrangement was investigated and the resulting temperature field is shown in Figure 12. It can be seen that such combination of internal and external cooling offer definite advantages, besides the considerable temperature reduction in highly stressed regions near the blade hub. The high radial temperature gradients in the blades that are present in the case of double path cooling with 3% coolant are avoided here. The computed temperature

field of Figure 12, shows mostly temperature gradients in the axial direction, with the exception of the rotor disk near the tip.

Although we did not intend to present a thermal stress analysis in this work, some discussion of the consequences of the temperature fields on the rotor stress distribution was presented. We would like to emphasize here again that the rotor dimensions and flow data were taken similar to Reference [5] with the exception that here, the rotor disk was extended radially outward up to the tip. Although this will not affect the temperature field, it would naturally result in a different stress distribution than in Reference [5]. Our computations showed that while internal cooling results in lower blade temperatures, particularly at the highly stressed regions near the hub, it also results in relatively high radial temperature gradients. This can augment the stresses produced by the centrifugal forces. The rotor external backside cooling on the other hand causes mostly axial temperature gradients with the exception of the rotor tip region where the centrifugal loading itself is insignificant. The combination of the two cooling schemes, namely that on the external rotor backside and in the internal single path, was found to result in the desired temperature reduction without the undesirable radial temperature gradient.

The stress field produced by centrifugal, thermal and aerodynamic loadings can be determined using one of the finite element stress analysis programs. The critical locations of possible creep, rupture or fatigue can be determined. Based on such information, it can be seen whether the external rotor backside cooling with its axial temperature gradient is preferable to the internal cooling, even if double the coolant mass flow is needed to achieve the same metal temperature reduction around the highly stressed blade regions.

CONCLUSIONS

A useful numerical technique has been developed to predict the three dimensional temperature field in the cooled rotor of a radial inflow turbine. It was found that the finite element method is especially suitable for handling the complicated surface boundaries encountered in the different cooling arrangements. The calculated temperatures obtained using the present method are in good agreement with other analytical methods involving more tedious and time consuming computations. The three dimensional temperature fields, calculated using the present analysis were also found to agree with the available experimental measurements.

REFERENCES

1. Esgar, J.B., "Turbine Cooling, Its Limitations and Its Future," AGARD CP 73-71, Paper No. 14.

2. Halls, G.A., "Nozzle Guide Vane Cooling - The State of the Art," AGARD CP 73-71, Paper No. 25.

3. Branger, M., Veil Cooling of Radial Flow Turbines. AiResearch Manufacturing Div., The Garrett Corp. Rep. 500. Final Report. Office of Naval Research Contract NONR 3685(00). Oct. 11, 1963. (AD 421888).

4. Petrick, E.N. and Smith, R.D., "Experimental Cooling of Radial Flow Turbines," ASME Paper No. 54-A-245. Presented at the Gas Turbine Power Division Annual Meeting, New York, New York, November 28 - December 3, 1954.

5. Calvert, G.S. and Okapuu, U.,"Design and Evaluation of High Temperature Radial Turbine," USAAVLABS Technical Report 68-69, January 1969.

6. Zienkiewicz, O.C. and Cheung, Y.K., The Finite Element Method in Structural and Continuum Mechanics, McGraw Hill, 1967.

7. Huebner, K.H., The Finite Element Method for Engineers, John Wiley and Sons, 1975.

8. Goldstein, S., Modern Developments in Fluid Dynamics, Vol. II, Dover Publications, Inc., 1965.

9. Ainley, D.G., "An Experimental Single Stage Air Cooled Turbine," Aircraft Engineering, Vol. 25, September 1953, pp. 269-276.

10. Miyazaki, H., "Combined Free and Forced Convective Heat Transfer and Fluid Flow in Rotating Curved Rectangular Tubes," Journal of Heat Transfer, February 1973, pp. 64-71.

11. Humble, L.V., Lowdermilk, W.H., and Desmon, L.G., "Measurements of Average Heat Transfer and Friction Coefficients for Subsonic Flow of Air in Smooth Tubes at High Surface and Fluid Temperatures," NACA Report No. 1020, 1951.

12. Haynes, C.M. and Owen, J.M., "Heat Transfer From a Shrouded Disk System With a Radial Outflow of Coolant," ASME Paper No. 74-GT-4. Presented at the Gas Turbine Conference, Zurich, Switzerland, March 31 - April 4, 1974.

13. Kreith, F., Doughman, E., and Kozlowski, H., "Mass and Heat Transfer From an Enclosed Rotating Disk With and Without Source Flow," Journal of Heat Transfer, Vol. 85, No. 2, May 1963, pp. 153-163.

14. Kreith, F., Principles of Heat Transfer, 2nd Edition, International Textbook Company, 1965.

15. Desai, C.S. and Abel, J.F., Introduction to the Finite Element Method, Van Nostrand Reinhold Co., 1972.

16. Emery, A.F. and Carson, W.W., "An Evaluation of the Use of the Finite-Element Method in the Computation of Temperature," Journal of Heat Transfer, Vol. 93, No. 2, May 1971, pp. 136-145.

17. Beaufait, F.W., Rowan Jr., W.H., Hoadley, P.G. and Hackett, R.M., Computer Methods of Structural Analysis, Prentice Hall, 1970.

18. Tabakoff, W. and Hamed, A., "Theoretical and Experimental Study of Flow Through Turbine Cascades with Coolant Flow Injection," AIAA Paper No. 75-843; presented to the AIAA 8th Fluid and Plasma Dynamics Conference, Hartford, Connecticut, June 16-18, 1975.

LIST OF SYMBOLS

C_f	Skin friction coefficient
C_p	Specific heat (Btu/lb°F)
D	Internal Cooling passage hydraulic diameter (ft)
{F}	A column vector representing the contribution of the convecting element to its thermal loading, Eq. (A-26)
g	Heat generation rate per unit volume (Btu/ft^{3}hr)
{G}	A column vector representing the contribution of the heat generation within an element to its thermal loading, Eq. (A-16)
h	Convective heat transfer coefficient (Btu/ft^{2}hr°F)
[H]	A tensor representing the convecting elements stiffness matrix, Eq. (A-26)
k	Coefficient of thermal conductivity (Btu/ft hr°F)
[K]	Overall thermal stiffness matrix
[k]	A tensor representing the conducting elements stiffness matrix, Eq. (A-16)
L	Cooling passage length
M	Total number of the finite elements in the solution domain
$\dot{m}$	Coolant mass flow rate (lb/sec)
{N}	The column vector of the elements interpolation functions
Nu	Nusselt number
$\bar{n}$	Outward normal unit vector from the rotor surface
p	Coolant passage perimeter (ft)
Pr	Prandtl number
{Q}	The column vector of a surface element thermal loading due to a specified amount of heat flux.

q	Heat flux density (Btu/ft^2 hr)
[R]	Overall thermal load vector
r	Radial distance along the rotor disk (ft)
Re	Reynolds number
S	Rotor surface
s	Finite element surface
T	Temperature (°F)
{T}	The column vector of nodal temperatures
V	Overall volume
v	Volume of finite element
Δ	Surface area of finite element
ν	Kinematic viscosity (ft^2/hr)
ω	Rotor angular velocity (radiance/hr)

Subscripts

c	Coolant flow
h	Referring to surfaces exchanging heat with the hot gas or coolant flow by convection
i,j, k,ℓ	Identify the various components of vectors or tensors, or nodes of a finite element
q	Referring to surfaces on which heat flux is specified including adiabatic surfaces
s	Rotor surface
∞	Flow conditions in hot gas or coolant flow

Superscripts

(e)	Refers to a finite element
t	Transpose of a tensor

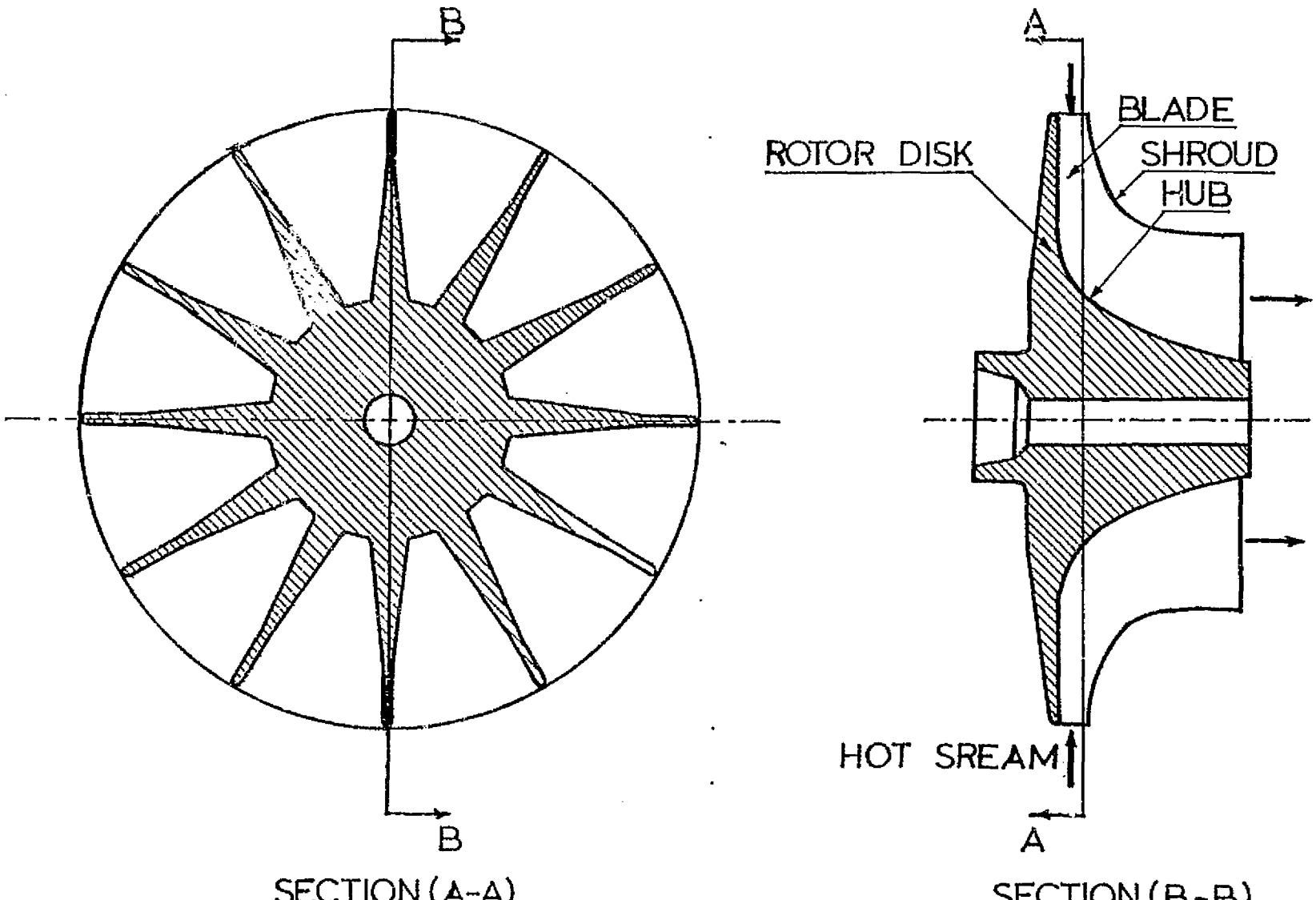

FIG. 1 A TYPICAL RADIAL INFLOW TURBINE ROTOR

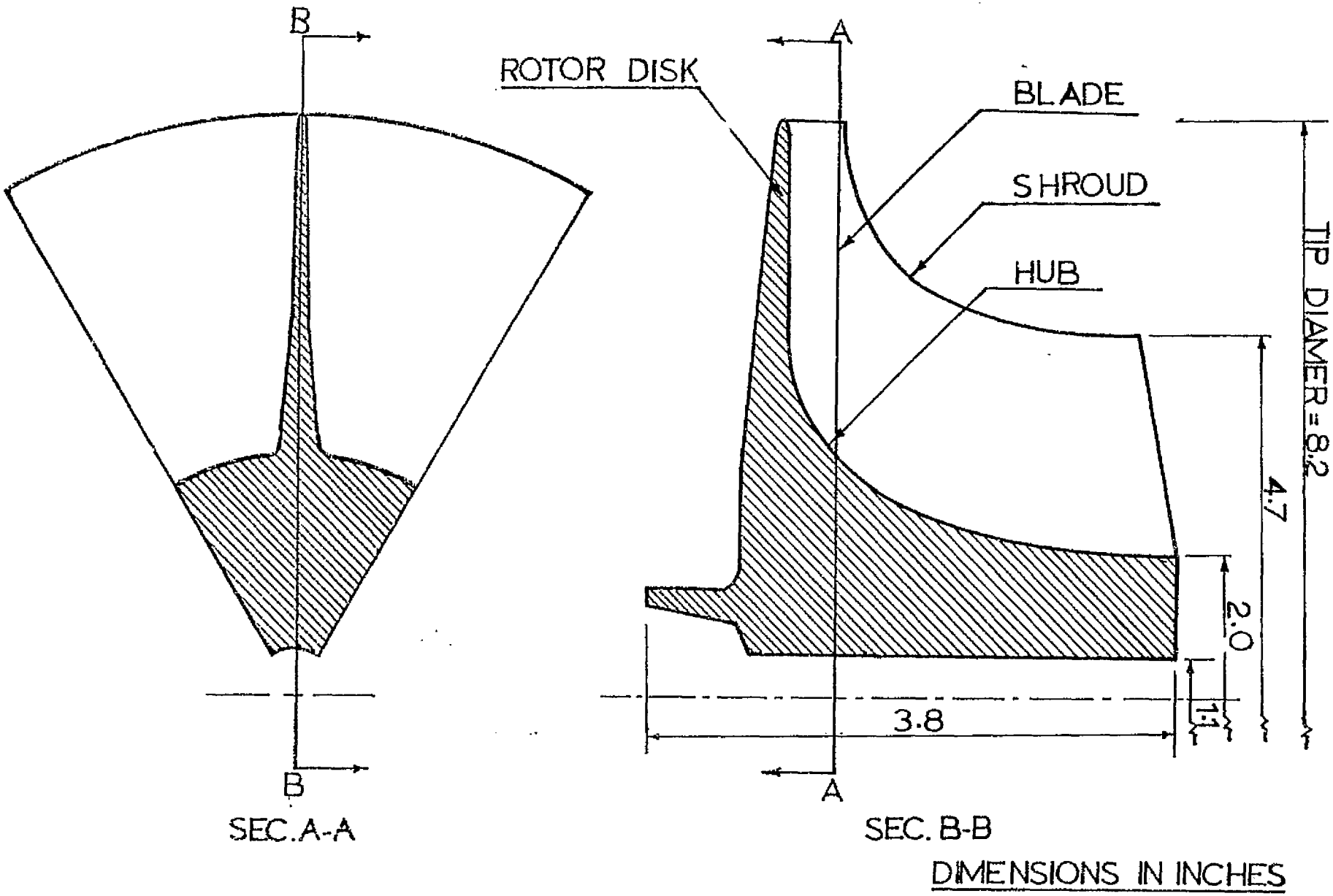

FIG. 2 ONE OF THE ROTOR TWELVE UNITS

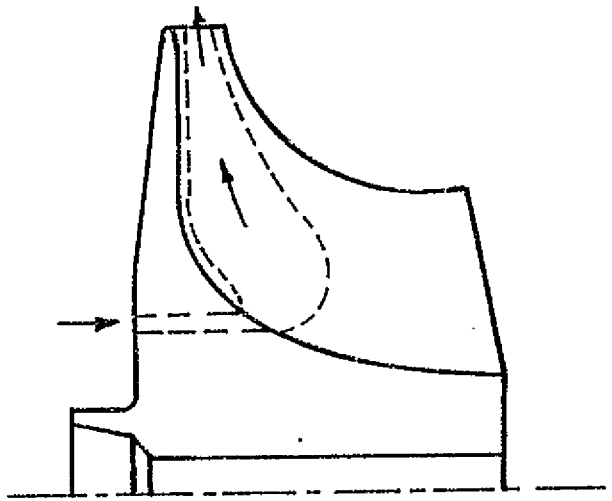

A) SINGLE PATH COOLING

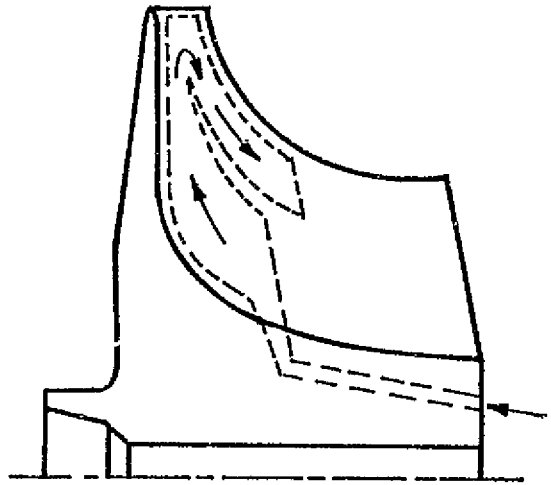

C) DOUBLE PATH COOLING

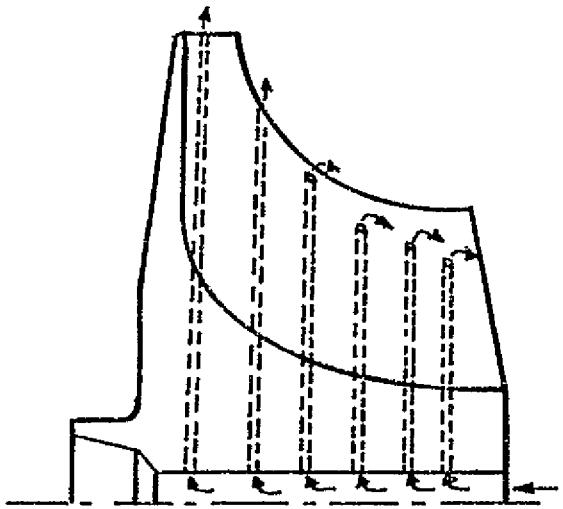

B) RADIAL PASSAGES COOLING

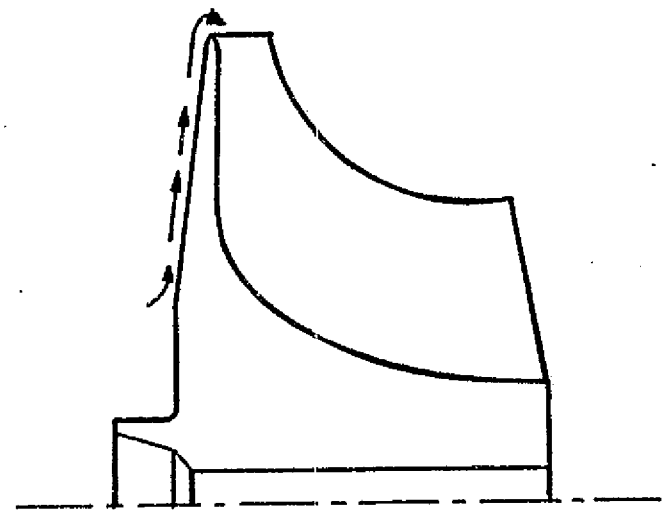

D) EXTERNAL DISC COOLING

FIG. 3 | ROTOR COOLING CONFIGURATIONS

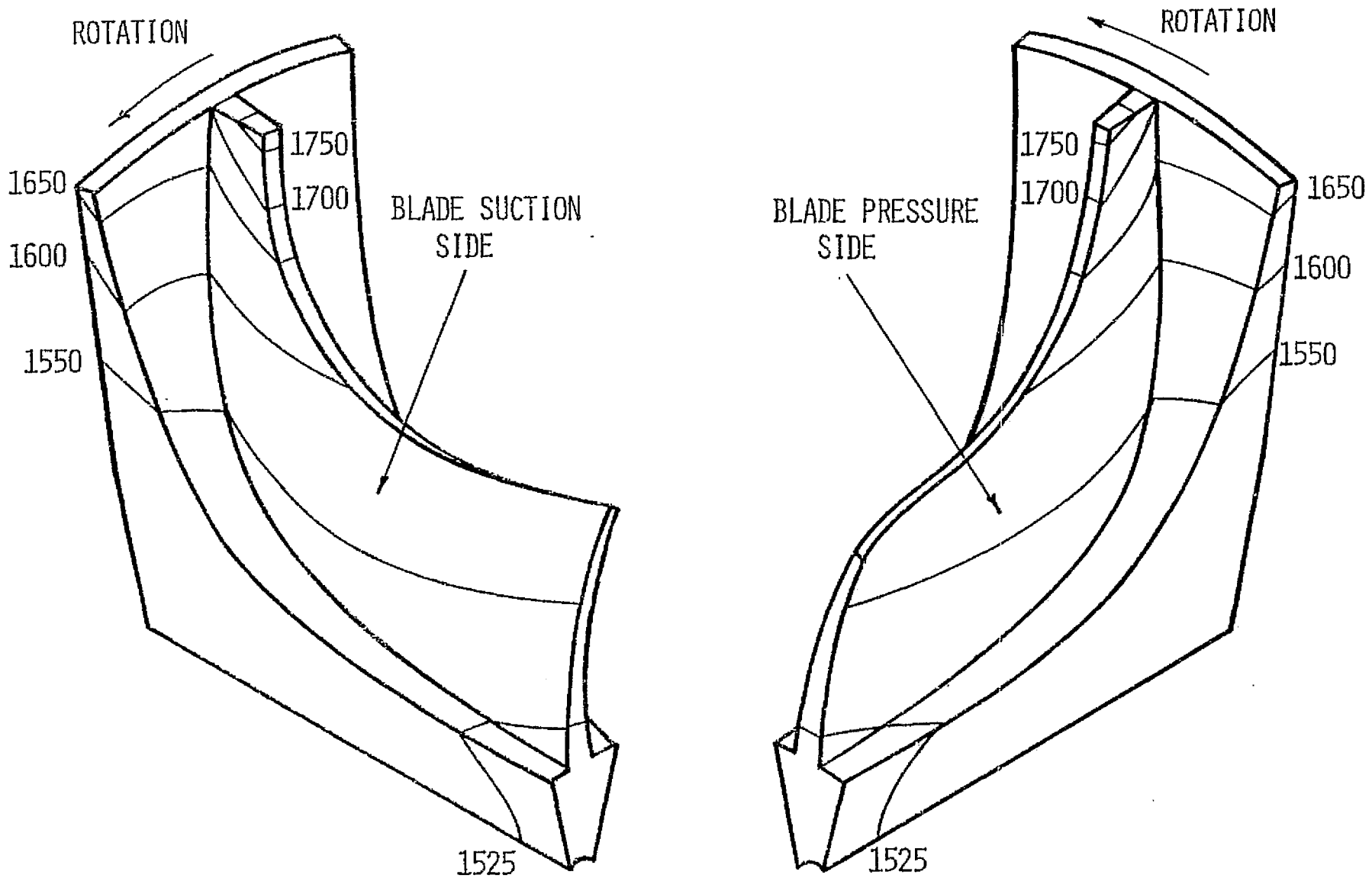

FIG. 4 ROTOR TEMPERATURE DISTRIBUTION WITHOUT COOLING

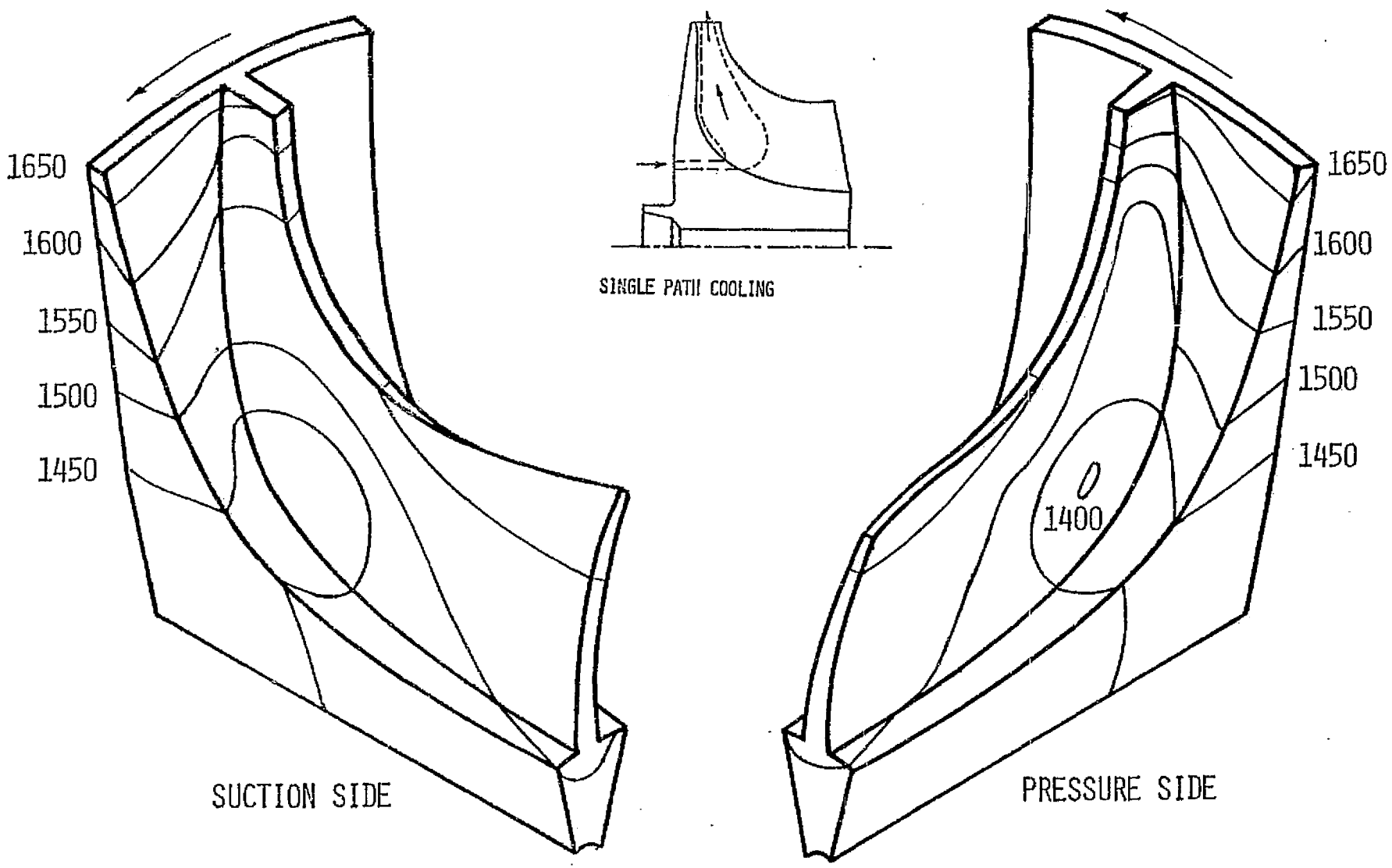

FIG. 5 | ROTOR TEMPERATURE DISTRIBUTION WITH 1.5% INTERNAL COOLING

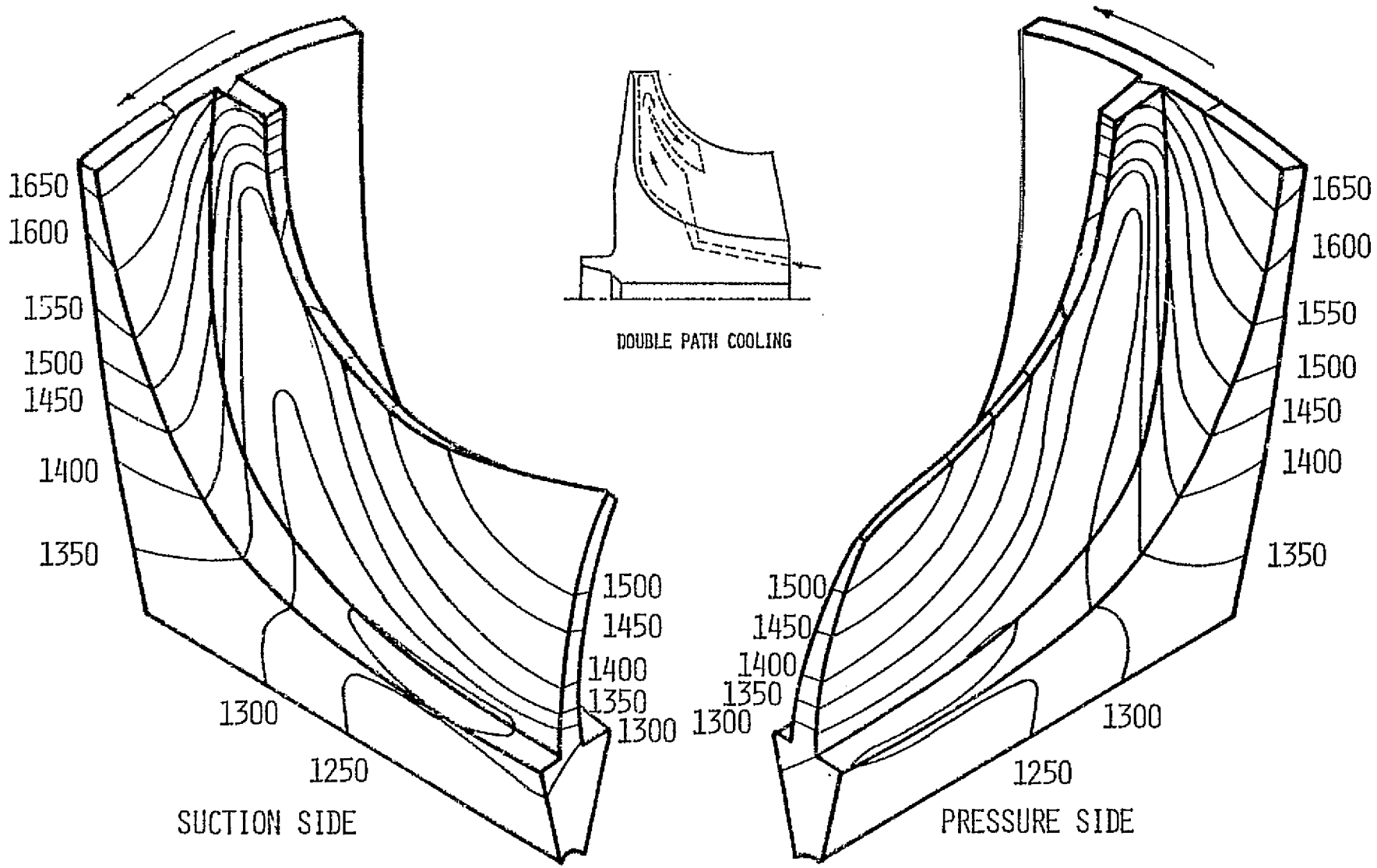

FIG. 6 ROTOR TEMPERATURE DISTRIBUTION WITH 3% INTERNAL COOLING

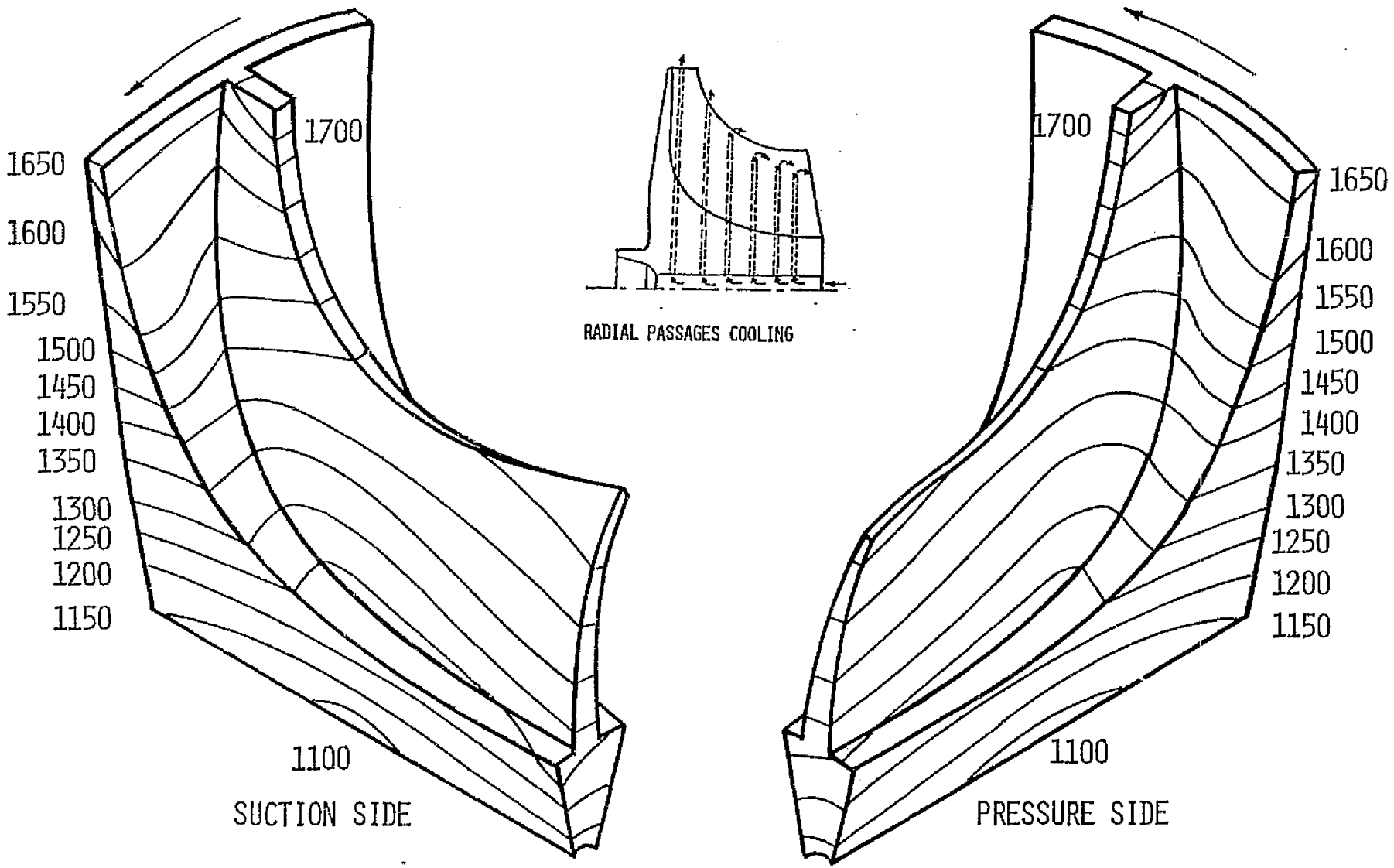

FIG. 7 ROTOR TEMPERATURE DISTRIBUTION WITH 1.5% INTERNAL COOLING

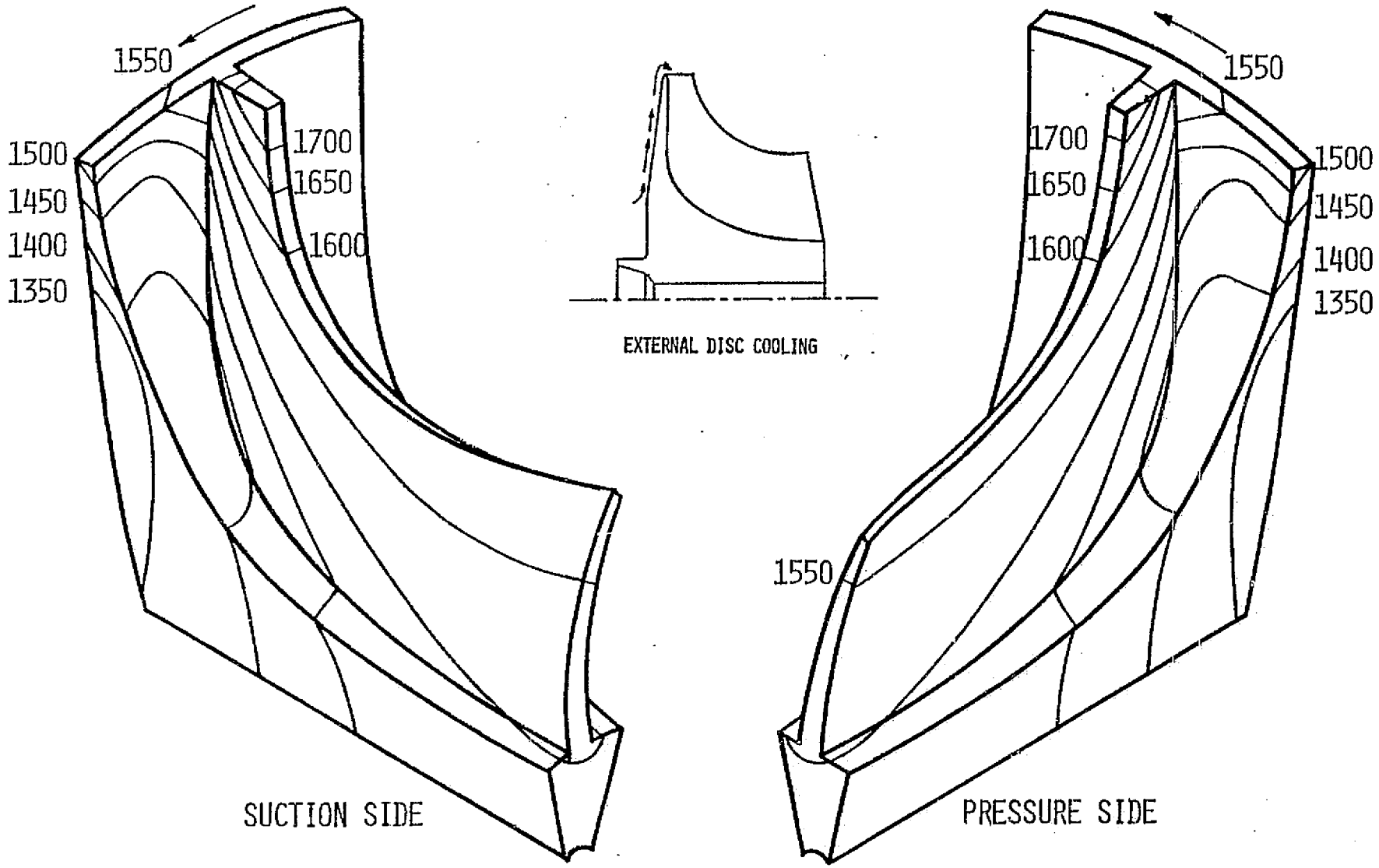

FIG. 8 ROTOR TEMPERATURE DISTRIBUTION WITH 1.5% EXTERNAL DISC COOLING

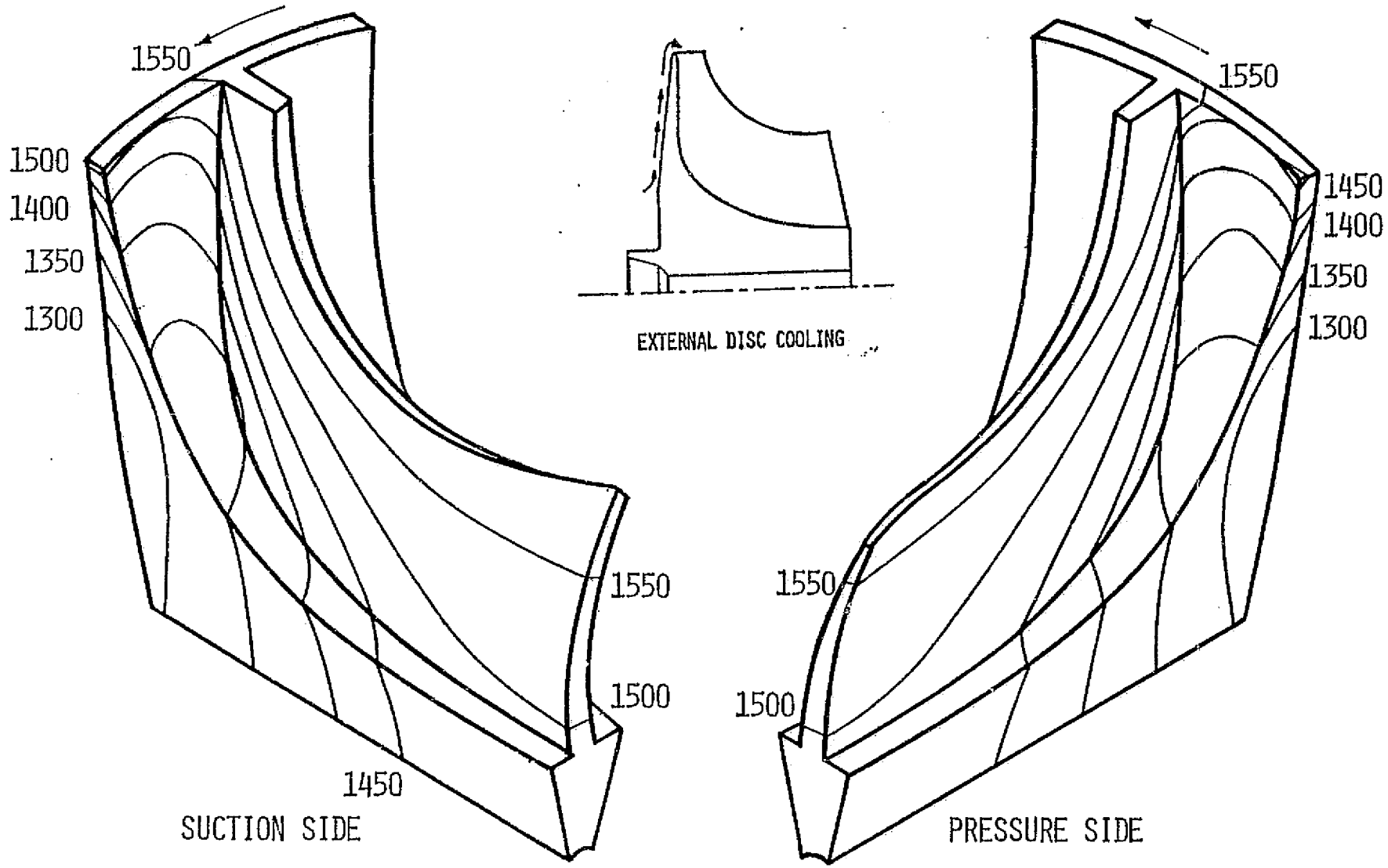

FIG. 9 ROTOR TEMPERATURE DISTRIBUTION WITH 3% EXTERNAL DISC COOLING

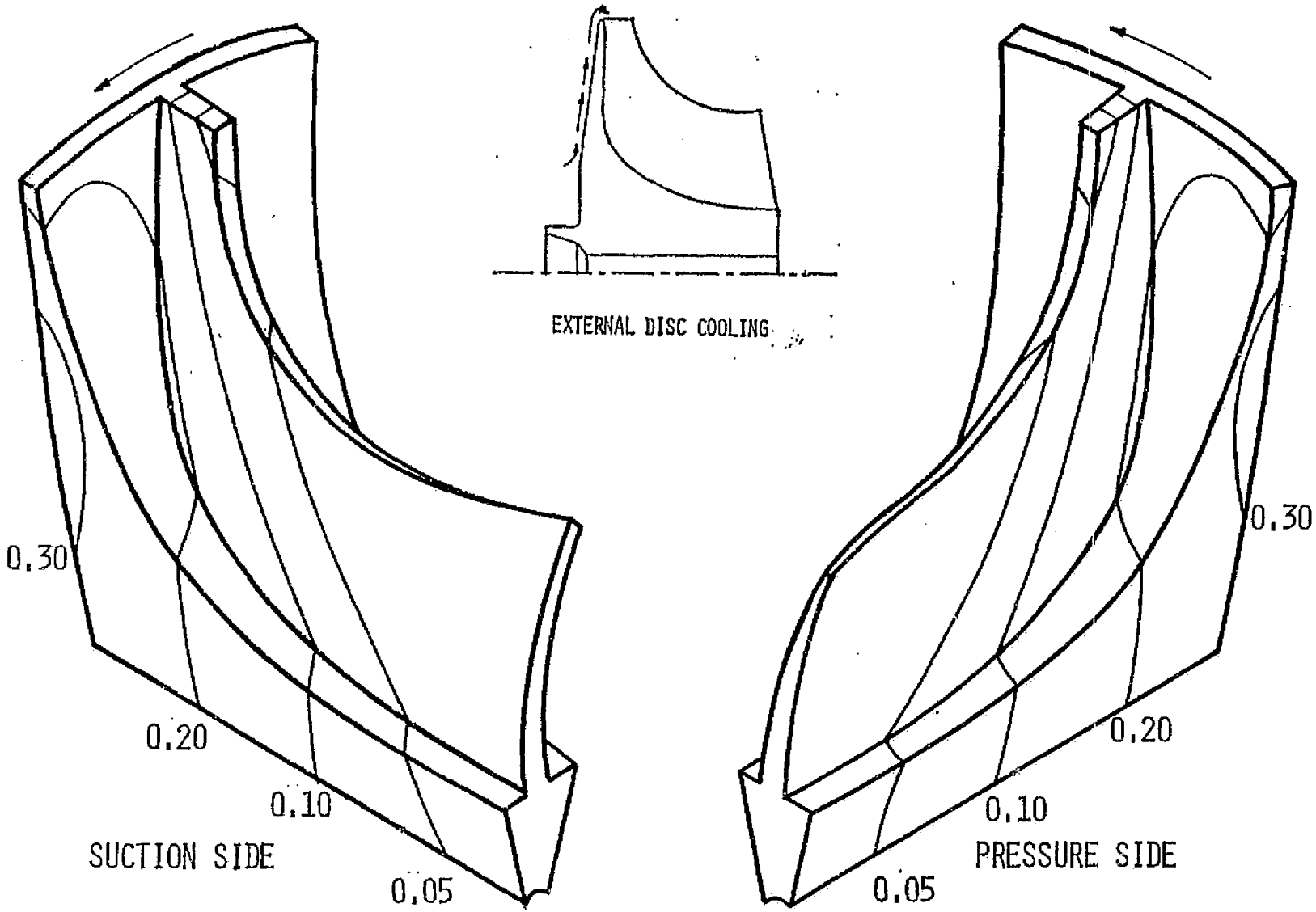

$$\eta = (T_{rh}-T_{rc})/(T_{rh}-T_c)$$

FIG. 10 COOLING EFFECTIVENESS WITH 1.5% EXTERNAL DISC COOLING

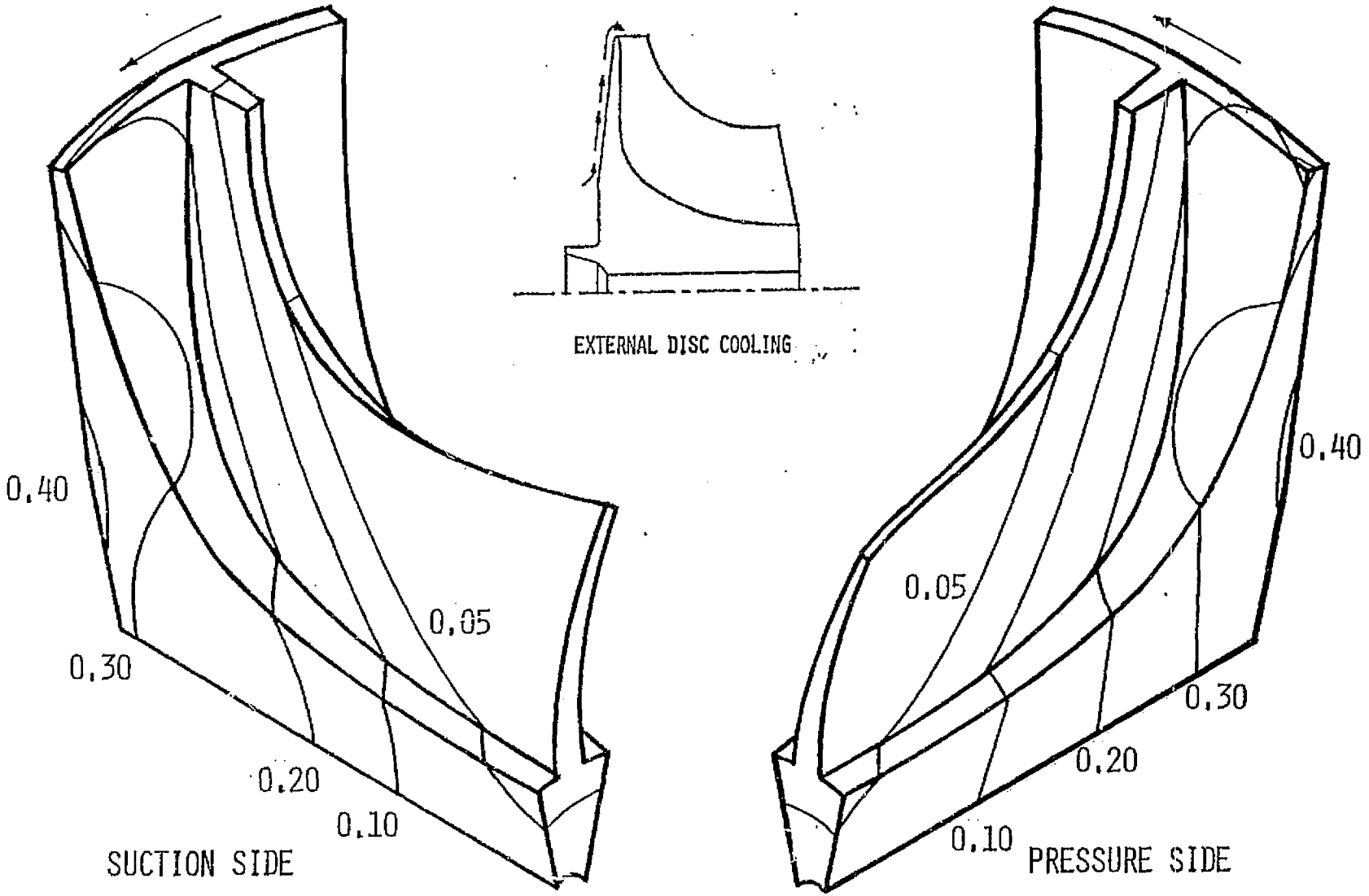

$\eta = (T_{rh}-T_{rc})/(T_{rh}-T_c)$

FIG. 11 COOLING EFFECTIVENESS WITH 3% EXTERNAL DISC COOLING

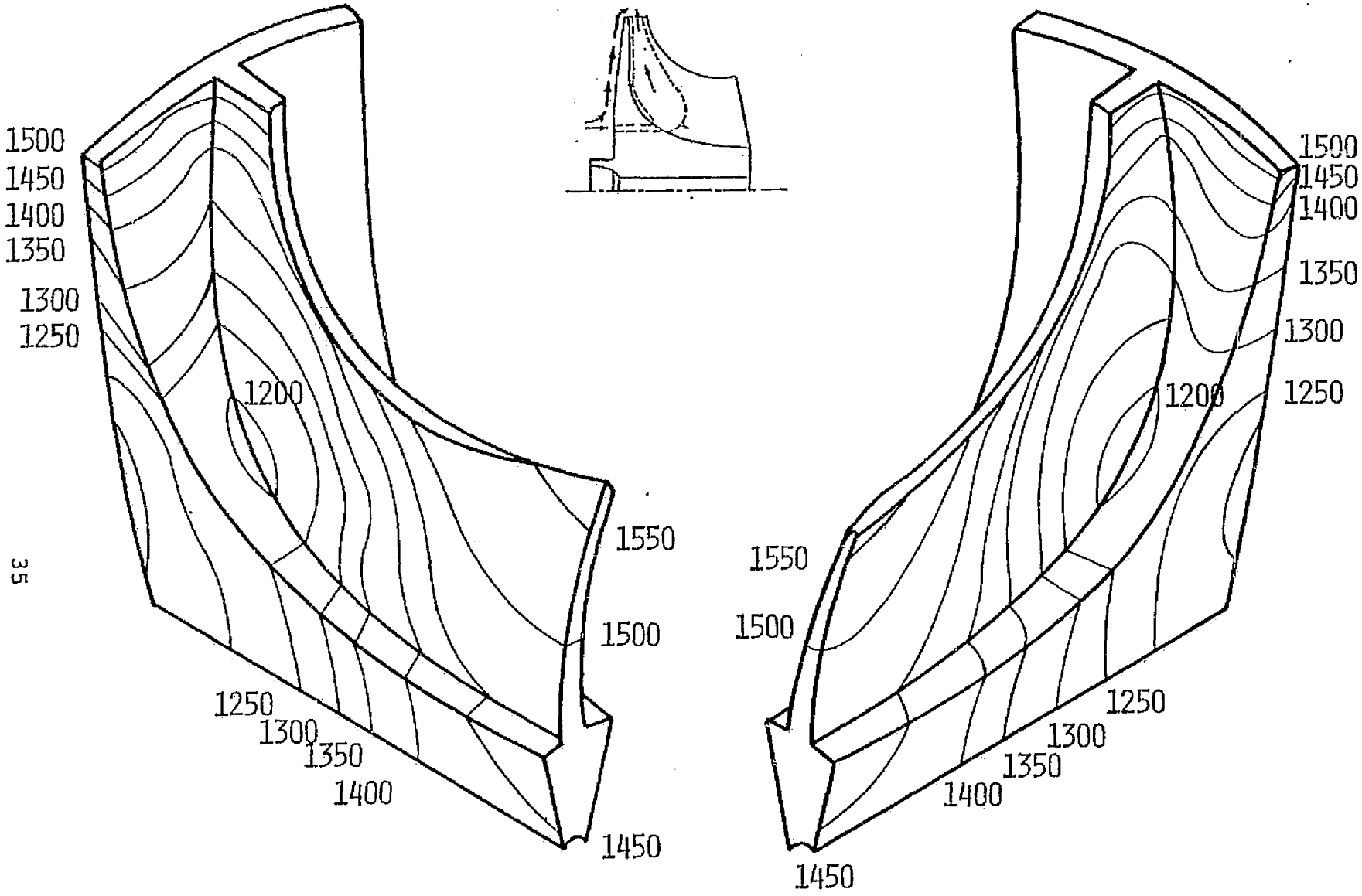

FIG. 12 ROTOR TEMPERATURE DISTRIBUTION WITH 1.5% EXTERNAL DISC COOLING AND 1.5% INTERNAL COOLING

APPENDIX A

ELEMENTS EQUATION

In this appendix, the elements equation will be derived for the simple four node tetrahedral element that was used in this analysis. The condition to stationize, the functional I, will be rewritten here for an element, as given by equation (16),

$$\frac{\partial I^{(e)}}{\partial T_i} = 0 \qquad i = 1, 2, \ldots r \tag{A-1}$$

When evaluating the integral over an element, it is more convenient to evaluate the different volume and surface integrals separately as follows:

$$I^{(e)} = I_v + I_{s_h} + I_{s_q} \tag{A-2}$$

where

$$I_v = \frac{1}{2} \int_v [k(\frac{\partial T^{(e)}}{\partial x})^2 + k(\frac{\partial T^{(e)}}{\partial y})^2 + k(\frac{\partial T^{(e)}}{\partial z})^2 - 2gT^{(e)}]dv \tag{A-3}$$

$$I_{s_h} = \frac{1}{2} \int_\Delta h(T^{(e)2} - 2T_\infty T^{(e)})ds \tag{A-4}$$

$$I_{s_q} = \int_\Delta q\, T^{(e)}\, ds \tag{A-5}$$

With the integrals in the above equations evaluated over the element's volume, v, and its corresponding surface areas, Δ. With the highest temperature derivative appearing under the integral, being of first order, the four node tetrahedral elements with linear interpolation functions, which are used here, are the simplest elements satisfying the compatability and the completeness requirements. Substituting equation (A-2) into equation (A-1), the elements equations can be written generally as:

$$\frac{\partial I_v}{\partial T_i} + \frac{\partial I_{s_h}}{\partial T_i} + \frac{\partial I_{s_q}}{\partial T_i} = 0 \qquad i = 1, 2, \ldots 4 \qquad \text{(A-6)}$$

where I_v, I_{s_h}, I_{s_q} are given by equations (A-3) to (A-5).

In the following, the different volume and surface integrals will be evaluated separately, with the temperature variation within the element, given by equation (13) which is rewritten here as

$$T^{(e)}(x,y,z) = \{N\}^t \{T\} \qquad \text{(A-7)}$$

Evaluation of the Volume Integral:

Using equation (A-3) we can write

$$\frac{\partial I_v}{\partial T_i} = \iiint_v \left[k \frac{\partial T^{(e)}}{\partial x} \frac{\partial}{\partial T_i} \left(\frac{\partial T^{(e)}}{\partial x}\right) + k \frac{\partial T^{(e)}}{\partial y} \frac{\partial}{\partial T_i} \left(\frac{\partial T^{(e)}}{\partial y}\right) + k \frac{\partial T^{(e)}}{\partial z} \frac{\partial}{\partial T_i} \left(\frac{\partial T^{(e)}}{\partial z}\right) - g \frac{\partial T^{(e)}}{\partial T_i}\right] dv \qquad i = 1,2,3,4 \qquad \text{(A-8)}$$

The derivatives in the above equation are evaluated with respect to each and every node associated with the element (e). Generally, the four numbers assigned to the nodes of the tetrahedral elements are arbiterary, however for simplicity, and without loss of generality, the nodes are assigned the numbers 1 to 4 in this derivation. The linear temperature variation within the four node tetrahedral elements, can be expressed as follows [8]:

$$T = N_i T_i \qquad i = 1,2,3,4 \qquad \text{(A-9)}$$

With $$N_i = \frac{1}{6v} (a_i + b_i x + c_i y + d_i z) \qquad \text{(A-10)}$$

where

$$a_i = \begin{vmatrix} x_j & y_j & z_j \\ x_k & y_k & z_k \\ x_\ell & x_\ell & x_\ell \end{vmatrix}$$

$$b_i = - \begin{vmatrix} 1 & y_j & z_j \\ 1 & y_k & z_k \\ 1 & y_\ell & z_\ell \end{vmatrix}$$

$$c_i = - \begin{vmatrix} x_j & 1 & z_j \\ x_k & 1 & z_k \\ x_\ell & 1 & z_\ell \end{vmatrix}$$

$$d_i = - \begin{vmatrix} x_j & y_j & 1 \\ x_k & y_k & 1 \\ x_\ell & y_\ell & 1 \end{vmatrix} \qquad \text{(A-11)}$$

and v is the volume of the tetrahedron defined by nodes i, j, k, ℓ in a right handed Cartesian coordinate system.

$$v = \frac{1}{6} \begin{vmatrix} 1 & x_i & y_i & z_i \\ 1 & x_j & y_j & z_j \\ 1 & x_k & y_k & z_k \\ 1 & x_\ell & y_\ell & z_\ell \end{vmatrix} \qquad \text{(A-12)}$$

The other constants are obtained through cycle permutation of the subscripts. It is possible to assume also a linear interpolation function for the heat source. This is not justified however in our problem since the heat source term was introduced to represent the heat absorption in a narrow cooling passage. Therefore, assuming g to be constant in a particular element, and substituting equation (A-9) into (A-8) we can write:

$$\frac{\partial I_v}{\partial T_i} = \int [k \{\frac{\partial N}{\partial x}\}^t \{T\} \frac{\partial N_i}{\partial x} + k \{\frac{\partial N}{\partial y}\}^t \{T\} \frac{\partial N_i}{\partial y} + k \{\frac{\partial N}{\partial z}\}^t \{T\} \frac{\partial N_i}{\partial z} - g N_i] dv \qquad \text{(A-13)}$$

The derivatives in the above integrations can be evaluated using equation (A-10)

$$\frac{\partial N_i}{\partial x} = \frac{b_i}{6v}$$

$$\frac{\partial N_i}{\partial y} = \frac{c_i}{6v}$$

$$\frac{\partial N_i}{\partial z} = \frac{d_i}{6v} \qquad \text{(A-14)}$$

where b_i, c_i and d_i are given by equation (A-11).

Substituting equation (A-14) into (A-13) we can write

$$\frac{\partial I_v}{\partial T_i} = k_{ij} T_j - G_i \qquad i,j = 1,2,3 \text{ and } 4 \qquad \text{(A-15)}$$

or

$$\{\frac{\partial I_v}{\partial T}\} = [k] \{T\} - \{G\} \qquad \text{(A-16)}$$

Where [k] is a four by four matrix in which

$$k_{ij} = \frac{k}{36v}(b_i b_j + c_i c_j + d_i d_j) \qquad \text{(A-17)}$$

and {G} is a column vector,

$$G_i = g\, v\, N_i \qquad \text{(A-18)}$$

Evaluation of the Surface Integrals:

Using equation (A-4), we can write

$$\frac{\partial I_{s_h}}{\partial T_i} = \int_\Delta (h\, T^{(e)} - T_\infty) \frac{\partial T^{(e)}}{\partial T_i}\, ds \qquad \text{(A-19)}$$

The linear temperature variation throughout the three node tetrahedral element is expressed as follows:

$$T^{(e)} = \{N\}^t \{T\} = N_i T_i \qquad i = 1, 2, 3 \qquad \text{(A-20)}$$

Therefore we can write

$$\frac{\partial I_{s_h}}{\partial T_i} = \int_\Delta (h\, \{N\}^t \{T\} - h\, T_\infty) N_i\, ds \qquad \text{(A-21)}$$

In performing the minimization, the convective heat transfer coefficient h, and the flow temperature are considered as invarients. Equation (A-21), thus involves integrals of terms such as N_i and $N_i N_j$, over the area of the triangular element. The values of such integrals are tabulated in various references [5, 6 and 15]. A general proof of the values of such integrals in one, two or three dimensional elements is given in Reference [A-1]. According to that reference, we can write for our surface elements:

$$\int_\Delta N_1^\alpha N_2^\beta N_3^\gamma\, ds \quad \frac{\alpha!\beta!\gamma!}{(\alpha+\beta+\gamma+2)!}\, 2\Delta \qquad \text{(A-22)}$$

Where Δ is the area of the triangular element. Using equation (A-20), we can write

$$\iint_{\Delta} h\, N_j N_i\, ds + \iint_{\Delta} h\, T_\infty\, N_i\, ds = H_{ij} - F_i$$

$$i,j = 1,\ 2 \text{ and } 3 \qquad \text{(A-23)}$$

where

$$H_{ij} = \frac{h\,\Delta}{12} \qquad i \neq j$$

$$= \frac{h\,\Delta}{6} \qquad i = j \qquad \text{(A-24)}$$

and $$F_i = h\, T_\infty\, \frac{\Delta}{3} \qquad i = 1,\ 2 \text{ and } 3 \qquad \text{(A-25)}$$

Using Equation (A-23) into equation (A-21) we can write

$$\frac{\partial I_{s_h}}{\partial T_i} = [H]\ \{T\} - \{F\} \qquad \text{(A-26)}$$

where [H] is a three by three square matrix, whose elements are given by equation (A-24), and {F} is a column vector whose elements are given by equation (A-25). The remaining term, $\partial I_{s_h}/\partial T_i$, was similarly evaluated taking the heat flux to be constant throughout the element, and using the linear temperature variation of equation (A-20).

$$\frac{\partial I_{s_q}}{\partial T_i} = \{Q\} = q\,\frac{\Delta}{3}\,\{I\} \qquad \text{(A-27)}$$

where $$Q_i = q\,\frac{\Delta}{3} \qquad i = 1,\ 2 \text{ and } 3 \qquad \text{(A-28)}$$

The surface area Δ of any triangle can be calculated if the three Cartesian coordinates of its vertices are known in a frame of reference. It is equal to half the magnitude of the vector resulting from the cross product of the vectors forming two sides of the triangle. The different surface and volume integrals over an element are given by equations (A-16), (A-26) and (A-27). If these equations are substituted into equations (A-1) and (A-2), the element equation can be expressed as:

$$[k]^{(e)} \{T\} = \{R\}^{(e)} \qquad \text{(A-29)}$$

which involves the contribution of the integral over the volume of the tetrahedral element and the contribution of the proper surface integral over its four triangular surfaces. In equation (A-29), $[k]^{(e)}$ is the four by four element stiffness matrix, $\{R\}^{(e)}$ is the column matrix representing the thermal loading, and $\{T\}$ the column matrix of the nodal temperatures. The thermal loading includes the contribution of the heat source (equation A-16), the convecting surface flow (equation A-26), and the specified heat flux q over an element surface (equation A-27).

Reference

(A-1) Eisenberg, M.A. and Malvern, L.E., "On Finite Element Integration in Natural Coordinates," International Journal of Numerical Methods in Engineering, Vol. 7, No. 4, October 1975, pp. 574-575.

APPENDIX B

COMPUTER PROGRAM

The numerical solution to the resulting set of linear simultaneous equations is obtained using the direct elimination approach in the subroutine CHOLES. It is called through the main program in which the computations of the stiffness matrix coefficients and the thermal load vector are carried out. This is accomplished through assembling the contribution of all the volume elements and the surface elements to equation (17). As explained in Appendix A, all the volume elements contribute to the global stiffness matrix. Those with heat sources or sinks contribute also to the thermal load vector. The convective surface elements contribute to both the overall stiffness matrix and the thermal load vector. If the heat flux is specified at some surface elements, they contribute only to the thermal load vector.

Although the elements equations were derived in Appendix A for tetrahedral elements, for the purpose of data preparation, the three dimensional body is discretized into pentahedral elements. This simplifies and reduces the size of the input data. Through computations in the main program each pentahedral element is further discretized into three tetrahedral elements as shown in Figure B. In the following, the program flow chart will be given, followed by the definition of the program symbols, a guide to input data preparation, then the program listing with sample input and output data.

THE VERTICES OF THE SHOWN PENTAHEDRAL ELEMENT
CAN BE FED IN THE PROGRAM INPUT AS:

1 2 3 4 5 6 OR
3 2 1 6 5 4 OR
5 4 6 2 1 3 ---ETC.

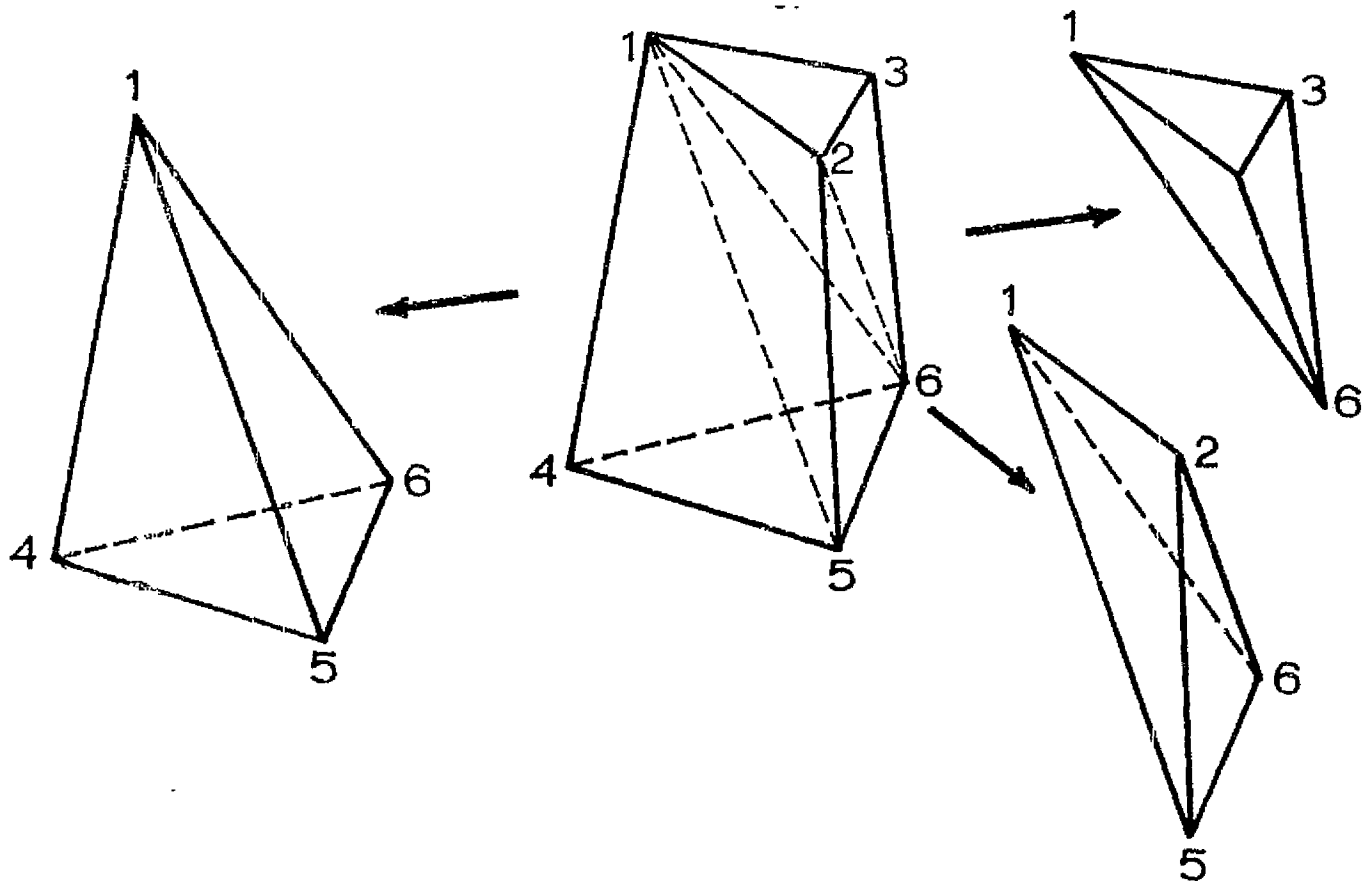

FIGURE B. DIVISION OF A TYPICAL PENTAHEDRAL ELEMENT INTO THREE TETRAHEDRAL ELEMENTS.

Program Flow Chart:

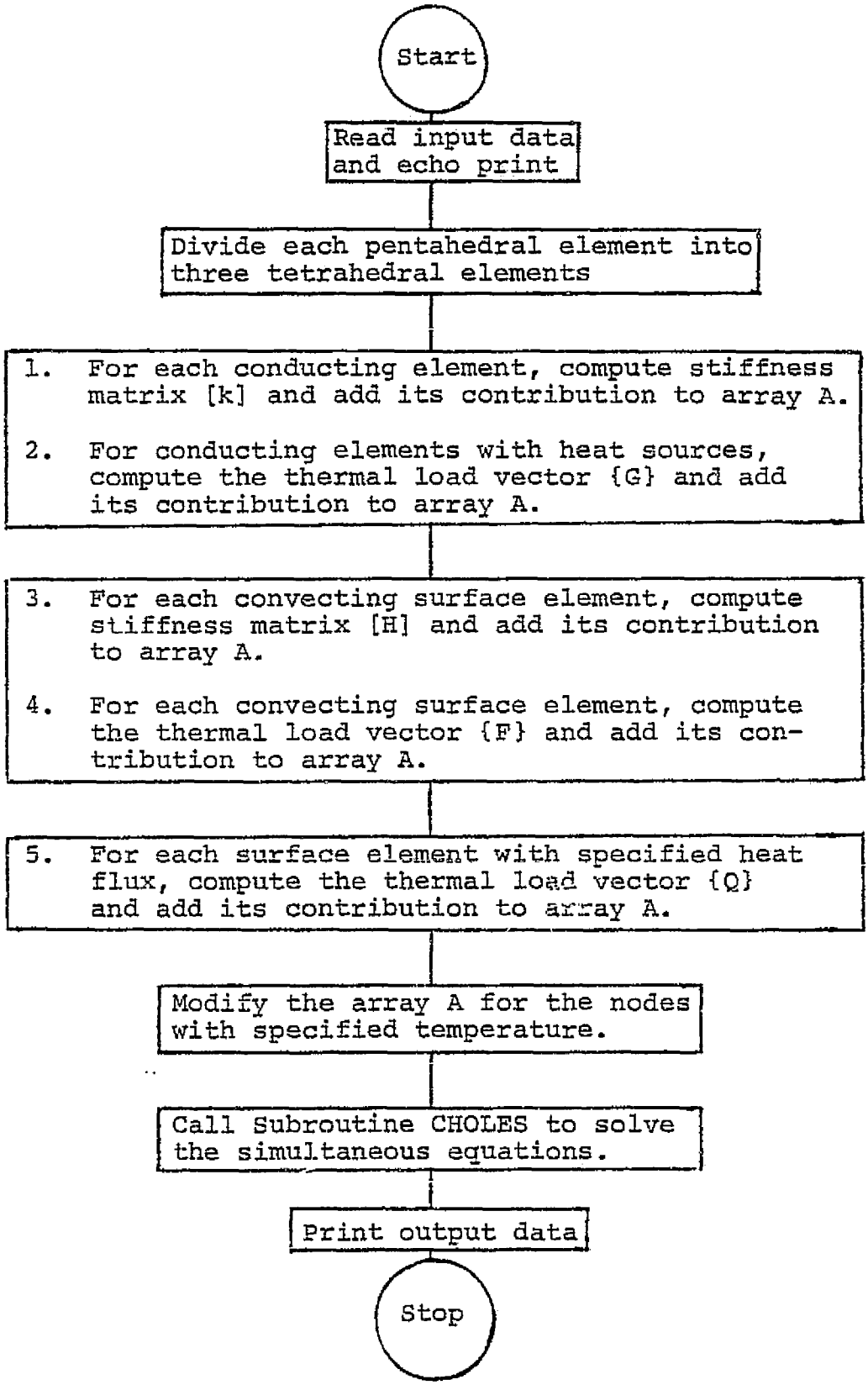

PROGRAM SYMBOLS

Symbol	Description
MTOT	Total number of nodes in the finite element model, M.
NTOT	Total number of pentahedral elements.
LTOT	Total number of triangular elements on convective surfaces.
ITOT	Total number of triangular elements on the body surface where heat flux is specified.
NSPEC	Total number of nodes where the temperature is specified.
NBW	Half band width of the stiffness matrix.
COND	Thermal conductivity of the body material, k.
IZ, NT	Code number, IZ, can be set equal to zero or unity. In the first case, only the input data and the final temperature distribution will be printed. In the second, NT coefficients determined in intermediate computations will also be printed.
TRANS	A coordinate multiplication factor in case the conversion of units is necessary.
X(I)	An array of the nodes x-coordinates.
Y(I)	An array of the nodes y-coordinates.
Z(I)	An array of the nodes z-coordinates.
KA,KB,KC KD,KE,KG	Numbers assigned to the vertices of a typical pentahedral element.
GEN	Rate of heat generated per unit volume within each pentahedral element.
LA,LB,LC	Numbers assigned to the vertices of a typical triangular surface element.

TINF	The environment temperature of a surface element.
HINF	The convective heat transfer coefficient at a surface element.
FLUX	Specified heat flux at a surface element.
NUM	The node numbers, where the temperature is specified.
TEMP	Specified temperature value.
T(I)	An array of the temperatures at all the body nodes.

The symbols of all program input data are explained above. The temporary storage variables were not defined. The one dimensional array A(I) is used to store the elements of the stiffness matrix lower band k_{ij} $(j \geq i)$, followed by the elements of the thermal load vector R_i $(i = 1, \ldots M)$.

Preparation of Input Data:

After the desired number of nodal points are placed throughout the three dimensional body and on its surfaces, they are designated the consecutive numbers between one and M. It is desirable that the discretization process simulate as closely as possible the original three dimensional body. The corners and the locations where there are abrupt changes in geometry or thermal boundary conditions, are obvious choices for nodal placement. At the regions where high temperature gradients are anticipated, finer discretization is employed.

Using the nodal points as vertices, the body is then divided into a number of pentahedral elements. The six numbers assigned to the vertices of each pentahedral element are inputed in an order such that the first three define a triangular base. The following three numbers define the vertices of the other base taken in the same order as the vertices of the first base (see Figure B). The coefficient of thermal conductivity and also the rate of heat generation (or absorption) if the element includes heat sources (or sinks) are also inputs for pentahedral elements.

The body surface is also divided into triangular elements using the surface nodal points. The input data of the surface elements depend upon the boundary conditions. The numbers of the nodes constituting each triangle are fed in the program input for each surface element. The corresponding local values of the film coefficient, h, and the environmental temperature, T_∞, are specified for elements on convective boundaries. The heat flux is an input for surface elements in the region of specified heat flow.

If the temperature is known at any nodal points, the numbers identifying such nodes and their specified temperatures are also given in the input. The program input format is explained in detail in the following section.

Type of Input	Input Data	Format	Number of Cards
Control data	MTOT, NTOT, LTOT ITOT, NSPEC, NBW	(6I5)	one
Control data	IZ, NT	(2I5)	one
Material properties & conversion factors	COND, TRANS	(2F10.0)	one
Geometrical	X(I)	(8 F10.0)	MTOT/8
	Y(I)	(8 F10.0)	MTOT/8
	Z(I)	(8 F10.0)	MTOT/8
Topology and properties of conducting elements	IA, IB, IC, ID, IE, IG, GEN	(6I5, F10.0)	NTOT
Convecting elements topology and boundary conditions	LAZ, LBZ, LCZ, TINF, HINF	(3I5, 2F10.0)	LTOT
Topology and boundary conditions of elements with specified heat flux	LAAZ, LABZ, LACZ, FLUX	(3I5, F10.0)	ITOT
Specified temperature nodes	NUM, TEMP	(I5, F10.0)	NSPEC

```
C
C
C
C                    A FORTRAN COMPUTER PROGRAM
C                    **************************
C
C       FOR SOLVING A THREE DIMENSIONAL HEAT TRANSFER PROBLEM
C       ****************************************************
C
C                 USING THE FINITE ELEMENT METHOD
C                 *******************************
C
C
C
      DIMENSION X(256),Y(256),Z(256),P(4,4),S(4,4),L(4),M(4),Q(4,4),V(4
     X,4),W(4,4),AA(4,4),PC(4),G(4),CC(4),SA(3,3),H(3,3),A(9281)
      CALL UNDFLW
      IPRNT=6
      READ(5,5001)MTOT,NTOT,LTOT,ITOT,NSPEC,NBW
      READ(5,5101)IZ,NT
      READ(5,5201)COND,TRANS
      MT=(MTOT*NBW)+MTOT-((NBW*(NBW+1))/2)
      MTP=MT+1
      MTF=MT+MTOT
      NBW1=NBW+1
      NBWP=NBW+2
C
C
C
C        MTOT =NO. OF NODES
C        NTOT =NO. OF THE BODY PENTAHEDRAL ELEMENTS
C        LTOT =NO. OF THE SURFACE ELEMENTS OF CONVECTION
C        ITOT =NO. OF THE SPECIFIED HEAT FLUX SURFACE ELEMENTS
C        NSPEC=NO. OF THE SPECIFIED TEMPERATURE NODES
C        NBW  =HALF BAND WIDTH OF THE STIFFNESS MATRIX
C        IZ   =CODE NUMBER FOR PRINTING A DESIRED NUMBER OF THE ARRAY
C              (A) ELEMENTS AFTER EACH MAJOR STEP(WHICH IS THE CASE IF
C              'IZ' IS SET EQUAL TO UNITY)
C        NT   =DESIRED NUMBER OF THE ARRAY (A) ELEMENTS TO BE PRINTED
C        COND =BODY MATERIAL THERMAL CONDUCTIVITY
C        TRANS=TRANSFORMATION FACTOR TO BE MULTIPLIED BY THE GIVEN
C              NODES COORDINATES TO TRANSFORM THEM INTO CENTIMETERS
C
C        THE ONE-DIMENSIONAL ARRAY (A) CONTAINS THE ELEMENTS OF THE
C        STIFFNESS MATRIX (S) LOWER BAND FOLLOWED BY THE ELEMENTS
C        OF THE R.H.S. VECTOR (C) IN THE SYSTEM OF EQUATIONS (A)(T)=(C)
C
C
C
      WRITE(6,6002)MTOT,NTOT,LTOT,ITOT,NSPEC,COND,NBW,IZ,TRANS,MT
C
C
C        READ AND PRINT THE NODAL COORDINATES
```

```
C
C
 3000 READ(5,5002)(X(I),I=1,MTOT)
      READ(5,5002)(Y(I),I=1,MTOT)
      READ(5,5002)(Z(I),I=1,MTOT)
      DO 1001  I=1,MTOT
      X(I)=TRANS*X(I)
      Y(I)=TRANS*Y(I)
      Z(I)=TRANS*Z(I)
 1001 CONTINUE
      WRITE(6,6001)
      DO 2 I=1,MTOT
      WRITE(6,6003)I,X(I),Y(I),Z(I)
    2 CONTINUE
C
C
C         ASSIGN ZERO VALUES TO ALL THE ELEMENTS OF THE ARRAY(A)
C
C
 1002 DO 3 I=1,MTF
      A(I)=0.0
   3  CONTINUE
      IF(NTOT.EQ.0) GO TO 14
C
C
C
C         THREE DIMENSIONAL HEAT CONDUCTION CALCULATIONS
C         **********************************************
C
C
C
      WRITE(6,6101)
      IW=0
      GO TO 1122
  100 IW=IW+1
      IF(IW.EQ.NTOT) GO TO 1009
C
C
C         READ AND PRINT THE NUMBERS ASSIGNED TO THE PENTAHEDRAL ELEMENT
C         VERTICES AND THE RATE OF HEAT GENERATED IN IT
C
C
 1122 READ(5,5005)IA,IB,IC,ID,IE,IG,GEN
      WRITE(6,6800) IA,IB,IC,ID,IE,IG,GEN
 2002 IM=1
C
C
C         BREAK THE PENTAHEDRAL ELEMENT UP INTO THREE TETRAHEDRAL
C         ELEMENTS AND CONSIDER EACH ONE OF THEM SEPARATELY
C
C
      NKA=IA
      NKB=ID
```

```
      NKC=IE
      NKD=IG
      GO TO 50
  300 NKA=IA
      NKB=IB
      NKC=IE
      NKD=IG
      GO TO 50
  400 NKA=IA
      NKB=IB
      NKC=IC
      NKD=IG
C
C
C         RE-ARRANGE THE VERTICES NUMBERS OF THE TETRAHEDRAL ELEMENT IN
C         AN ASCENDING ORDER
C
C
   50 IF(NKA-NKB) 1050,1050,1051
 1050 JK1=NKA
      JK2=NKB
      GO TO 1150
 1051 JK1=NKB
      JK2=NKA
 1150 IF(NKC-NKD)1060,1060,1061
 1060 JK3=NKC
      JK4=NKD
      GO TO 1160
 1061 JK3=NKD
      JK4=NKC
 1160 IF(JK1-JK3)1070,1070,1071
 1070 KK1=JK1
      KK2=JK2
      KK3=JK3
      KK4=JK4
      GO TO 1170
 1071 KK1=JK3
      KK2=JK4
      KK3=JK1
      KK4=JK2
 1170 IF(KK2-KK4)1080,1080,1081
 1080 LK1=KK1
      LK2=KK2
      LK3=KK3
      LK4=KK4
      GO TO 1180
 1081 LK1=KK1
      LK2=KK4
      LK3=KK3
      LK4=KK2
 1180 IF(LK2-LK3)1090,1090,1190
 1090 KA=LK1
      KB=LK2
```

```
      KC=LK3
      KD=LK4
      GO TO 2100
 1190 KA=LK1
      KB=LK3
      KC=LK2
      KD=LK4
 2100 WRITE(6,6004)KA,KB,KC,KD
C
C
C         CALCULATE THE TETRAHEDRAL ELEMENT CONTRIBUTION MATRIX,(K)
C
C
 2003 P(1,1)=1.0
      P(1,2)=X(KA)
      P(1,3)=Y(KA)
      P(1,4)=Z(KA)
      P(2,1)=1.0
      P(2,2)=X(KB)
      P(2,3)=Y(KB)
      P(2,4)=Z(KB)
      P(3,1)=1.0
      P(3,2)=X(KC)
      P(3,3)=Y(KC)
      P(3,4)=Z(KC)
      P(4,1)=1.0
      P(4,2)=X(KD)
      P(4,3)=Y(KD)
      P(4,4)=Z(KD)
      COF=(P(2,2)*((P(3,3)*P(4,4))-(P(3,4)*P(4,3))))-(P(3,2)*((P(2,3)*P(
     X4,4))-(P(2,4)*P(4,3))))+(P(4,2)*((P(2,3)*P(3,4))-(P(2,4)*P(3,3))))
      COG=(P(1,2)*((P(3,3)*P(4,4))-(P(3,4)*P(4,3))))-(P(3,2)*((P(1,3)*P(
     X4,4))-(P(1,4)*P(4,3))))+(P(4,2)*((P(1,3)*P(3,4))-(P(1,4)*P(3,3))))
      COH=(P(1,2)*((P(2,3)*P(4,4))-(P(2,4)*P(4,3))))-(P(2,2)*((P(1,3)*P(
     X4,4))-(P(1,4)*P(4,3))))+(P(4,2)*((P(1,3)*P(2,4))-(P(1,4)*P(2,3))))
      COP=(P(1,2)*((P(2,3)*P(3,4))-(P(2,4)*P(3,3))))-(P(2,2)*((P(1,3)*P(
     X3,4))-(P(1,4)*P(3,3))))+(P(3,2)*((P(1,3)*P(2,4))-(P(1,4)*P(2,3))))
      AD=COF-COG+COH-COP
      VOL=(ABS(AD))/6.0
      CT=VOL*COND
      CTT=GEN/3.0
      CALL MINV(P,4,AF,L,M)
      S(1,1)=0.0
      S(1,2)=0.0
      S(1,3)=0.0
      S(1,4)=0.0
      S(2,1)=0.0
      S(2,2)=1.0
      S(2,3)=0.0
      S(2,4)=0.0
      S(3,1)=0.0
      S(3,2)=0.0
      S(3,3)=1.0
```

```
      S(3,4)=0.0
      S(4,1)=0.0
      S(4,2)=0.0
      S(4,3)=0.0
      S(4,4)=1.0
      CALL MPRD(S,P,Q,4,4,0,0,4)
      CALL MTRA(P,V,4,4,0)
      CALL MPRD(V,Q,W,4,4,0,0,4)
      DO 1000 I=1,4
      DO 2000 J=1,4
      AA(I,J)=CT*W(I,J)
 2000 CONTINUE
 1000 CONTINUE
C
C
C        COMPUTE THE ORDERS OF THE ARRAY (A) ELEMENTS TO BE INFLUENCED
C        BY ADDING THE MATRIX (K) TO THE ARRAY (A)
C
C
      NQ=1
      KN=KA
      NSUM=0
      GO TO 8872
 8871 NSUM=0
      IF(NQ.EQ.2) KN=KB
      IF(NQ.EQ.3) KN=KC
      IF(NQ.EQ.4) KN=KD
      IF(NQ.EQ.5) GO TO 1929
 8872 DO 9971 J=1,KN
      NSUM=NSUM+J
 9971 CONTINUE
      IDG=NSUM
      IF(KN-NBWP) 7765,7766,7766
 7765 I=IDG
      GO TO 9973
 7766 NACC=0
      DO 7768 K=NBWP,KN
      NACC=NACC+K-NBWP+1
 7768 CONTINUE
      I=IDG-NACC
 9973 A(I)=A(I)+AA(NQ,NQ)
      NQ=NQ+1
      GO TO 8871
 1929 ICODE=1
      NU=KB
      NV=KA
      GO TO 3260
 3225 NU=KC
      NV=KA
      GO TO 3260
 3226 NU=KC
      NV=KB
      GO TO 3260
```

```
 3227 NU=KD
      NV=KA
      GO TO 3260
 3228 NU=KD
      NV=KB
      GO TO 3260
 3229 NU=KD
      NV=KC
 3260 LNU=NU-1
      NADD=0
      DO 3261 J=1,LNU
      NADD=NADD+J
 3261 CONTINUE
      NDG=NADD
      IF(NU-NBWP)1980,1984,1981
 1980 I=NDG+NV
      GO TO 1982
 1981 JACC=0
      DO 1983 K=NBWP,LNU
      JACC=JACC+K-NBWP+1
 1983 CONTINUE
      I1=NDG-JACC
      I=I1+NV-NU+NBWP-1
      GO TO 1982
 1984 I=NDG+NV-1
 1982 GO TO (3262,3263,3264,3265,3266,3267),ICODE
C
C
C        ADD THE TETRAHEDRAL ELEMENT CONTRIBUTION MATRIX (K) TO THE
C        ARRAY (A) IN THE PROPER PLACES CALCULATED BEFORE
C
C
 3262 A(I)=A(I)+AA(2,1)
      GO TO 3367
 3263 A(I)=A(I)+AA(3,1)
      GO TO 3367
 3264 A(I)=A(I)+AA(3,2)
      GO TO 3367
 3265 A(I)=A(I)+AA(4,1)
      GO TO 3367
 3266 A(I)=A(I)+AA(4,2)
      GO TO 3367
 3267 A(I)=A(I)+AA(4,3)
 3367 ICODE=ICODE+1
      GO TO (9000,3225,3226,3227,3228,3229,8844),ICODE
C
C
C        COMPUTE THE TETRAHEDRAL ELEMENT COLUMN VECTOR (G) RESULTING
C        FROM THE HEAT GENERATED WITHIN THIS ELEMENT
C
C
 8844 XC=(X(KA)+X(KB)+X(KC)+X(KD))/4.0
      YC=(Y(KA)+Y(KB)+Y(KC)+Y(KD))/4.0
```

```
      ZC=(Z(KA)+Z(KB)+Z(KC)+Z(KD))/4.0
      PC(1)=1.0
      PC(2)=XC
      PC(3)=YC
      PC(4)=ZC
      CALL MPRD(V,PC,G,4,4,0,0,1)
      DO 9 I=1,4
      CC(I)=CTT*G(I)
    9 CONTINUE
      KAP=MT+KA
      KBP=MT+KB
      KCP=MT+KC
      KDP=MT+KD
      A(KAP)=A(KAP)+CC(1)
      A(KBP)=A(KBP)+CC(2)
      A(KCP)=A(KCP)+CC(3)
      A(KDP)=A(KDP)+CC(4)
C
C
C        RETURN TO CONSIDER ANOTHER TETRAHEDRAL ELEMENT
C
C
      IM=IM+1
      GO TO (9000,300,400,100),IM
 1009 IF(IZ.EQ.0) GO TO 14
C
C
C        PRINT PORTION OF THE ARRAY (A) AFTER CONSIDERING ALL THE BODY
C        ELEMENTS
C
C
      WRITE(6,6005)
      DO 12 I=1,NT
      WRITE(6,6006)I,A(I)
   12 CONTINUE
   14 IF(LTOT.EQ.0) GO TO 23
C
C
C
C              HEAT CONVECTION BOUNDARY CONDITION
C              **********************************
C
C
C
      WRITE(6,6009)
 4010 DO 15 K=1,LTOT
C
C
C        READ THE NUMBERS ASSIGNED TO THE CONVECTIVE TRIANGULAR ELEMENT
C        VERTICES AND THE VALUES OF BOTH THE ENVIRONMENT TEMPERATURE
C        AND THE HEAT TRANSFER COEFFICIENT
C
C
```

```
      READ(5,5006)LAZ,LBZ,LCZ,TINF,HINF
C
C
C         RE-ARRANGE THE NUMBERS IN AN ASCENDING ORDER
C
C
      IF(LAZ-LBZ) 4012,4012,4013
 4012 LA1=LAZ
      LB1=LBZ
      LC1=LCZ
      GO TO 4014
 4013 LA1=LBZ
      LB1=LAZ
      LC1=LCZ
 4014 IF(LA1-LC1) 4015,4015,4016
 4015 LA2=LA1
      LB2=LB1
      LC2=LC1
      GO TO 4017
 4016 LA2=LC1
      LB2=LB1
      LC2=LA1
 4017 IF(LB2-LC2) 4018,4018,4019
 4018 LA=LA2
      LB=LB2
      LC=LC2
      GO TO 4020
 4019 LA=LA2
      LB=LC2
      LC=LB2
 4020 WRITE(6,6010)LA,LB,LC,TINF,HINF
C
C
C         COMPUTE THE CONTRIBUTION MATRIX (H) OF THE CONVECTIVE ELEMENT
C
C
 4021 ALA=((Y(LB)-Y(LA))*(Z(LC)-Z(LA))-(Y(LC)-Y(LA))*(Z(LB)-Z(LA)))
      ALB=((X(LB)-X(LA))*(Z(LC)-Z(LA))-(X(LC)-X(LA))*(Z(LB)-Z(LA)))
      ALC=((X(LB)-X(LA))*(Y(LC)-Y(LA))-(X(LC)-X(LA))*(Y(LB)-Y(LA)))
      ZLA=(ABS(ALA))**2.0
      ZLB=(ABS(ALB))**2.0
      ZLC=(ABS(ALC))**2.0
      AREA=0.5*((ZLA+ZLB+ZLC)**0.5)
      SA(1,1)=2.0
      SA(1,2)=1.0
      SA(1,3)=1.0
      SA(2,1)=1.0
      SA(2,2)=2.0
      SA(2,3)=1.0
      SA(3,1)=1.0
      SA(3,2)=1.0
      SA(3,3)=2.0
      CINF=(AREA*HINF)/12.0
```

```
      DO 16 I=1,3
      DO 17 J=1,3
      H(I,J)=CINF*SA(I,J)
   17 CONTINUE
   16 CONTINUE
C
C
C        CALCULATE THE ORDES OF THE ARRAY (A) ELEMENTS TO WHICH THE
C        CONVECTIVE ELEMENT CONTRIBUTE
C
C
      NQ1=1
      KN1=LA
      NSUM=0
      GO TO 4111
 4110 NSUM=0
      IF(NQ1.EQ.2) KN1=LB
      IF(NQ1.EQ.3) KN1=LC
      IF(NQ1.EQ.4) GO T   4400
 4111 DO 4112 J=1,KN1
      NSUM=NSUM+J
 4112 CONTINUE
      IDG1=NSUM
      IF(KN1-NBWP) 4113,4114,4114
 4113 I=IDG1
      GO TO 4117
 4114 NAC1=0
      DO 4115 J=NBWP,KN1
      NAC1=NAC1+J-NBWP+1
 4115 CONTINUE
      I=IDG1-NAC1
 4117 A(I)=A(I)+H(NQ1,NQ1)
      NQ1=NQ1+1
      GO TO 4110
 4400 ICOD1=1
      NU1=LB
      NV1=LA
      GO TO 4401
 4501 NU1=LC
      NV1=LA
      GO TO 4401
 4502 NU1=LC
      NV1=LB
 4401 LNU1=NU1-1
      NAD1=0
      DO 4402 J=1,LNU1
      NAD1=NAD1+J
 4402 CONTINUE
      NDG1=NAD1
      IF(NU1-NBWP) 4403,4404,4405
 4403 I=NDG1+NV1
      GO TO 4407
 4405 JAC1=0
```

```
      DO 4406 J=NBWP,LNU1
      JAC1=JAC1+J-NBWP+1
 4406 CONTINUE
      J1=NDG1-JAC1
      I=J1+NV1-NU1+NBWP-1
      GO TO 4407
 4404 I=NDG1+NV1-1
C
C
C        ADD THE CONTRIBUTION OF THE CONVECTIVE ELEMENT TO THE PROPER
C        ELEMENTS OF THE ARRAY (A)
C
C
 4407 GO TO (4601,4602,4603),ICOD1
 4601 A(I)=A(I)+H(2,1)
      GO TO 4904
 4602 A(I)=A(I)+H(3,1)
      GO TO 4904
 4603 A(I)=A(I)+H(3,2)
 4904 ICOD1=ICOD1+1
      GO TO(9000,4501,4502,4605),ICOD1
C
C
C        COMPUTE THE CONTRIBUTION VECTOR (F) OF THE CONVECTIVE ELEMENT
C
C
 4605 DINF=(HINF*TINF*AREA)/3.0
      LAS=LA+MT
      LBS=LB+MT
      LCS=LC+MT
C
C
C        ADD (F) TO THE ARRAY (A) IN THE PROPER PLACES
C
C
      A(LAS)=A(LAS)+DINF
      A(LBS)=A(LBS)+DINF
      A(LCS)=A(LCS)+DINF
   15 CONTINUE
      IF(IZ.EQ.0) GO TO 23
      WRITE(6,6011)
      DO 21 I=1,NT
      WRITE(6,6012)I,A(I)
   21 CONTINUE
   23 IF(ITOT.EQ.0) GO TO 29
C
C
C
C            SPECIFIED HEAT FLUX BOUNDARY CONDITION
C            **************************************
C
C
C
```

```
      WRITE(6,6015)
      DO 24 K=1,ITOT
C
C
C        READ THE NUMBERS ASSIGNED TO THE SPECIFIED HEAT FLUX TRIANGULAR
C        ELEMENT AND THE SPECIFIED VALUE OF THE HEAT FLUX AT THAT
C        ELEMENT
C
C
      READ(5,5007)LAAZ,LABZ,LACZ,FLUX
C
C
C        RE-ARRANGE THE VERTICES NUMBERS IN AN ASCENDING ORDER
C
C
      IF(LAAZ-LABZ)9012,9012,9013
 9012 LAA1=LAAZ
      LAB1=LABZ
      LAC1=LACZ
      GO TO 9014
 9013 LAA1=LABZ
      LAB1=LAAZ
      LAC1=LACZ
 9014 IF(LAA1-LAC1)9015,9015,9016
 9015 LAA2=LAA1
      LAB2=LAB1
      LAC2=LAC1
      GO TO 9017
 9016 LAA2=LAC1
      LAB2=LAB1
      LAC2=LAA1
 9017 IF(LAB2-LAC2)9018,9018,9019
 9018 LAA=LAA2
      LAB=LAB2
      LAC=LAC2
      GO TO 9020
 9019 LAA=LAA2
      LAB=LAC2
      LAC=LAB2
 9020 WRITE(6,6016)LAA,LAB,LAC,FLUX
C
C
C        COMPUTE THE ELEMENT CONTRIBUTION VECTOR (Q)
C
C
      BLA=((Y(LAB)-Y(LAA))*(Z(LAC)-Z(LAA))-(Y(LAC)-Y(LAA))*(Z(LAB)-Z(LAA
     X))**2.0
      BLB=((X(LAB)-X(LAA))*(Z(LAC)-Z(LAA))-(X(LAC)-X(LAA))*(Z(LAB)-Z(LAA
     X))**2.0
      BLC=((X(LAB)-X(LAA))*(Y(LAC)-Y(LAA))-(X(LAC)-X(LAA))*(Y(LAB)-Y(LAA
     X))**2.0
      AREA=0.5*((BLA+BLB+BLC)**0.5)
      FIX=(AREA*FLUX)/3.0
```

```
      LA1=LAA+MT
      LB1=LAB+MT
      LC1=LAC+MT
      A(LA1)=A(LA1)+FIX
      A(LB1)=A(LB1)+FIX
      A(LC1)=A(LC1)+FIX
   24 CONTINUE
      IF(IZ.EQ.0) GO TO 29
      WRITE(6,6017)
      DO 28 I=1,NT
      WRITE(6,6018)I,A(I)
   28 CONTINUE
   29 IF(NSPEC.EQ.0) GO TO 43
C
C
C
C              SPECIFIED TEMPERATURE BOUNDARY CONDITION
C              ****************************************
C
C
C
      WRITE(6,6019)
      DO 30 I=1,NSPEC
C
C
C        READ AND PRINT THE NODE NUMBER AND ITS SPECIFIED TEMPERATURE
C        VALUE
C
C
      READ(5,5008)NUM,TEMP
      WRITE(6,6020)NUM,TEMP
C
C
C        MODIFY THE ARRAY (A) BY SUBSTITUTING THE SPECIFIED TEMPERATURE
C        VALUE IN THE RESULTING SET OF SIMULTANEOUS EQUATIONS
C
C
      IM=NUM-1
      IP=NUM+1
      NUM1=NUM+MT
      IP1=MT+IP
      IF(NUM.EQ.1) A(NUM)=1.0
      A(NUM1)=TEMP
      LSUM=0
      DO 2450 J=1,NUM
      LSUM=LSUM+J
 2450 CONTINUE
      LDG=LSUM
      IF(NUM.EQ.1) GO TO 2457
      IF(NUM-NBW1) 2451,2451,2452
 2451 A(LDG)=1.0
      LDGM=LDG-NUM+1
      GO TO 2454
```

```
2452 ISUM=0
     DO 2453 J=NBWP,NUM
     ISUM=ISUM+J-NBWP+1
2453 CONTINUE
     LDG=LDG-ISUM
     A(LDG)=1.0
     LDGM=LDG-NBW
     GO TO 2455
2454 MT2=MT+IM
     DO 2456 J=MTP,MT2
     K=J-MTP+LDGM
     A(J)=A(J)-(TEMP*A(K))
     A(K)=0.0
2456 CONTINUE
     GO TO 2556
2455 MPLC=MTP+NUM-NBW1
     MT2=MT+IM
     DO 2555 J=MPLC,MT2
     K=J-MPLC+LDGM
     A(J)=A(J)-(TEMP*A(K))
     A(K)=0.0
2555 CONTINUE
2556 IF(NUM.EQ.MTOT) GO TO 30
     JUD=MTOT-NUM
     IF(JUD.LT.NBW) GO TO 6560
     IF(NUM-NBW1) 2457,2458,2458
2457 NUM2=NBW1-NUM
     I3=LDG
     DO 6461 K=1,NUM2
     I3=I3+NUM+K-1
     I4=NUM1+K
     A(I4)=A(I4)-(TEMP*A(I3))
     A(I3)=0.0
6461 CONTINUE
     IJ=I4
     IF(NUM.EQ.1) GO TO 3020
     DO 6462 K=1,IM
     I3=I3+NBW
     I4=IJ+K
     A(I4)=A(I4)-(TEMP*A(I3))
     A(I3)=0.0
6462 CONTINUE
3020 DO 7010 J=MTP,MTF
     WRITE(6,7110)J,A(J)
7110 FORMAT(4X,I3,4X,E12.5)
7010 CONTINUE
     GO TO 30
2458 I6=LDG
     DO 6463 K=1,NBW
     I6=I6+NBW
     I7=NUM1+K
     A(I7)=A(I7)-(TEMP*A(I6))
     A(I6)=0.0
```

```
 6463 CONTINUE
      GO TO 30
 6560 I8=LDG
      DO 6561 K=1,JUD
      I8=I8+NBW
      I9=NUM1+K
      A(I9)=A(I9)-(TEMP*A(I8))
      A(I8)=0.0
 6561 CONTINUE
   30 CONTINUE
      IF(IZ.EQ.0) GO TO 43
      WRITE(6,1985)
      DO 1986 I=1,NT
      WRITE(6,1987)I,A(I)
 1986 CONTINUE
C
C
C        SOLVE THE FINAL SET OF SIMULTANEOUS EQUATIONS
C
C
   43 CALL CHOLES(A,MTOT,NBW1,0,1,IPRNT,&9000)
C
C
C        PRINT THE TEMPERATURE VALUES AT ALL THE BODY NODES
C
C
      WRITE(6,6023)
      DO 45 I=MTP,MTF
      J=I-MT
      WRITE(6,6024)J,A(I)
   45 CONTINUE
 5001 FORMAT(6I5)
 5101 FORMAT(2I5)
 5201 FORMAT(2F10.0)
 5002 FORMAT(8F10.0)
 5005 FORMAT(6I5,F10.0)
 5006 FORMAT(3I5,F10.0)
 5007 FORMAT(3I5,F10.0)
 5008 FORMAT(I5,F10.0)
 6002 FORMAT(55X,'MTOT=',I3/55X,'NTOT=',I3/55X,'LTOT=',I3/55X,'ITOT=',I
     X3/55X,'NSPEC=',I3/55X,'COND=',F5.2/55X,'NBW=',I3/55X,'IZ=',I1/55X
     X,'TRANS=',F10.5///45X,'SIZE OF THE STIFFNESS MATRIX=',I6)
 6001 FORMAT(1H1//50X,'NODAL POINTS COORDINATES'/30X,'NODE NO.',13X,'X
     X',15X,'Y',15X,'Z'//)
 6003 FORMAT(32X,I3,10X,F10.8,5X,F10.4,5X,F10.4)
 6101 FORMAT(1H1/43X,'THREE DIMENSIONAL HEAT CONDUCTION CALCULATIONS'/4
     X3X,' ',46('*')/43X,' ',46('*')//61X,'INPUT DATA'/61X,' ',10('*')/
     X/)
 6800 FORMAT(30X,6(4X,I3),4X,F10.4)
 6004 FORMAT(81X,4(4X,I3))
 6005 FORMAT(1H1//54X,'PORTION OF THE ARRAY (A)'/28X,'AFTER ADDING THE C
     XONTRIBUTION OF THE CONDUCTIVE FINITE ELEMENTS'//)
 6006 FORMAT(54X,I5,4X,E10.3)
```

```
6009 FORMAT(1H1/50X,'HEAT CONVECTION BOUNDARY CONDITION'/49X,' ',
    X34('*')//61X,'INPUT DATA'/61X,' ',10('*')//)
6010 FORMAT(45X,3(4X,I3),6X,F6.1,4X,F5.1)
6011 FORMAT(1H1//54X,'PORTION OF THE ARRAY (A)'/28X,'AFTER ADDING THE C
    XONTRIBUTION OF THE CONVECTIVE FINITE ELEMENTS'//)
6012 FORMAT(54X,I5,4X,E10.3)
6015 FORMAT(1H1/47X,'SPECIFIED HEAT FLUX BOUNDARY CONDITION'/47X,' ',3
    X8('*')/47X,' ',38('*')//61X,'INPUT DATA'/61X,' ',10('*')//)
6016 FORMAT(50X,3(4X,I3),6X,F5.1)
6017 FORMAT(1H1//54X,'PORTION OF THE ARRAY (A)'/33X,'AFTER ADDING THE C
    XONTRIBUTION OF THE SPECIFIED HEAT FLUX ELEMENTS'//)
6018 FORMAT(54X,I3,4X,E10.3)
6019 FORMAT(1H1//30X,'INPUT DATA FOR THE SPECIFIED TEMPERATURE NODES'//
    X)
6020 FORMAT(50X,I3,4X,F6.1)
1985 FORMAT(1H1//54X,'PORTION OF THE ARRAY (A)'/41X,'AFTER INTRODUCING
    XTHE SPECIFIED NODAL TEMPERATURES'//)
1987 FORMAT(56X,I5,E12.5)
6023 FORMAT(1H1/51X,'FINAL TEMPERATURE DISTRIBUTION'/50X,' ',30('*')/
    X50X,' ',30('*')//52X,'NODE NUMBER',5X,'TEMPERATURE'/51X,' ',11('*'
    X),4X,' ',11('*')/)
6024 FORMAT(55X,I5,11X,F12.6)
9000 STOP
     END
```

```
      SUBROUTINE CHOLES(B,N,MM,IB,NT,IPRNT,*)
      REAL*8   S1,T1
      DIMENSION B(1)
C
C
C        (B) IS THE ARRAY CONTAINING THE ELEMENTS OF THE LOWER HALF BAND
C            OF THE STIFFNESS MATRIX (S)
C        N   =NO. OF THE UNKNOWN NODAL TEMPERATURES
C        MM  =HALF BAND WIDTH OF THE STIFFNESS MATRIX +1
C        S1,T1 ARE TEMPORARY DOUBLE PRECESION VARIABLES
C
C
      MUD = MM-1
      NS = MUD*MM/2
      NM = N*MM-NS
      IF(NT-1)30,30,31
C
C
C        BEGIN CHOLESKY ALGORITHM FOR FACTORING THE MATRIX
C
C
   30 DO 20 J = 1,N
      IF(J-MUD) 1,1,2
    2 IN =J-MUD
      L= IN +(J-MM)*MUD +NS
      GO TO 7
    1 IN= 1
      L= IN +(J-1)*J/2
    7 IF (J -N+MUD)103,103,105
  105 M5 =N
      GO TO 104
  103 M5 = J+MUD
  104 S1 = 0.0
      J1 = J-1
      J2 = J+1
      IF(J1)4,4,3
    3 DO 6 K = IN,J1
      T1 = B(L)
      S1 =S1 + T1**2
    6 L=L +1
    4 T1=B(L)
      IF(T1-S1 .LT.0.) GO TO 100
      T1 =DSQRT(T1 - S1)
      B(L) = T1
      IF(J-N)19,20,20
   19 DO 18 I= J2 ,M5
      SUM = 0.0
      IF(I-MUD)68,68,71
   71 IN = I-MUD
      LL = IN + (I-MM)*MUD +NS
      GO TO 5
   68 IN = 1
      LL = IN + (I-1)*I /2
```

```
    5 IF(J1)18,18,8
    8 IF(IN -J1) 53,53,18
   53 DO 17 K = IN,J1
      LM = L+K-J
      SUM = SUM + B(LL)*B(LM)
   17 LL = LL +1
   18 B(LL) = (B(LL)-SUM) /B(L)
   20 CONTINUE
   31 NR = IB +1
C
C
C        BEGIN FORWARD SUBSTITUTION
C
C
      NB =NM +1
      DO 65 K =1,NR
      B(NB) =B(NB)/B(1)
      DO 60 I = 2,N
      IF (I -MUD) 21,21,22
   22 IN = I -MM
      KS = IN* MUD +NS
      MS =MUD
      GO TO 27
   21 IN = 0
      MS = I-1
      KS = MS*I /2
   27 SUM = 0.0
      DO 61 J= 1,MS
      JR = J+IN
      L  = JR +KS
      JR  = JR + NB - 1
   61 SUM = SUM +B(L)  *B(JR)
      ID = I + KS
   60 B(JR+1) = (B(JR+1) -SUM)/B(ID)
   65 NB = NB +N
C
C
C        BEGIN BACKWARD SUBSTITUTION
C
C
      NS =NM + N
      DO 75  K = 1,NR
      B(NB) = B(NB) /B(NM)
      DO 80 II = 2,N
      I = N -II +1
      IF(I-MUD)41,41,95
   95 ID =I +(I-MM)* MUD +NS
      GO TO 42
   41 ID =I +(I-1)*I /2
   42 IF(I-N+MM) 43,43,45
   45 MS =II-1
      GO TO 76
   43 MS = MUD
```

```
 76 SUM =0.0
    DO 81 J =1,M5
    JR = I +J
    IF(JR-MUD)98,98,99
 99 L = I +(JR-MM)*MUD+NS
    GO TO 82
 98 L = I +(JR-1)*JR/2
 82 JR=NB-N+JR
 81 SUM =SUM + B(L)*B(JR)
    JR =NB -N +I
 80 B(JR)= (B(JR)-SUM) /B(ID)
 75 NB =NB +N
    RETURN
100 WRITE(IPRNT,901)
901 FORMAT(1H1,' THE MATREX IS NOT POSITIVE DEFINITE IN THIS PROBLEM *
   X)
    RETURN1
    END
```